ABSTRACT

Title of Document:	QUALITY AND RELIABILITY OF ELASTOMER SOCKETS
	Leoncio D. Lopez, Doctor of Philosophy (Ph.D.), 2009
Directed By:	Chair Professor and Director, Michael G. Pecht, Department of Mechanical Engineering

Integrated Circuit (IC) sockets provide hundreds to thousands of electrical interconnects in enterprise servers, where quality and reliability are critical for customer applications. The evaluation of IC sockets, according to current industry practices, relies on the execution of stress loads and stress levels that are defined by standards, having no consideration to the physics of failure (PoF), target operating environment, or contact resistance behavior over time. In a similar manner, monitoring of contact resistance during system operation has no considerations to the PoF or environmental conditions.

In this dissertation a physics of failure approach was developed, to model the reliability of elastomer sockets that are used in an enterprise server application. The temperature and relative humidity environment, at the IC socket contact interface, were characterized as a function of external environmental conditions and microprocessor activity. The study applied state-of-the-art health monitoring

techniques to assess thermal gradients on the IC socket assembly, and to establish an operating profile that could be used for the development of a PoF model.

A methodology was developed for modeling and monitoring contact resistance of electrical interconnects. The technique combined a PoF model with the Sequential Probability Ratio Test (SPRT). In the methodology the resistance behavior is characterized as a function of temperature. The effective a-spot radius was extracted from the characterization data and modeled with a power-law. A PoF model was developed to estimate the resistance of an elastomer contact, based on the effective a-spot radius and the ambient temperature. The methodology was experimentally demonstrated with a temperature cycle test of the elastomer socket. During the evaluation the difference between estimated and observed resistance values were tested with the SPRT. The technique was shown to be very accurate for modeling contact resistance, and to be highly sensitive for the detection of resistance degradation.

A qualitative reliability model was developed for the mean contact resistance of an elastomer socket, using fundamental material properties and user defined failure criteria. To derive the model, the resistance behavior of contacts under nominal mechanical load was studied as a function of time and temperature. The elastomer contact was shown to have a very complex resistance behavior, which was modeled by multiple statistical distributions. It was shown that elastomer sockets, in spite of experiencing stress relaxation at the macroscale (elastomer), can exhibit decreases in contact resistance, a result of stress redistribution at the microscale (Ag particles), which increases Ag-Ag particle stress and the effective contact area.

QUALITY AND RELIABILITY OF ELASTOMER SOCKET

By

Leoncio D. Lopez

Dissertation submitted to the Faculty of the Graduate School of the
University of Maryland, College Park, in partial fulfillment
of the requirements for the degree of
Doctor of Philosophy
2009

Advisory Committee:
Professor Michael G. Pecht, Chair
Professor Donald Barker
Associate Professor Peter Sandborn
Associate Professor David Bigio
Professor Herbert Rabin, Dean's Representative

Preface

"In the discovery of secret things, and in the investigation of hidden causes, stronger reasons are obtained from sure experimentations and demonstrated arguments, than from probable conjectures and the opinions of philosophical speculators."

- William Gilbert

Dedication

This is dedicated to my dear wife Cindy, and to my children Paige, Adriana, and Braeden. Cindy's support, patience, and continuous encouragement will never be forgotten. There is no doubt that the sacrifices made by my family made this research possible.

This work is also dedicated to my father, Leoncio Lopez, and my mother, Rebeca Lopez. They taught me well as a child the value of an education.

Acknowledgements

My sincere gratitude goes to Dr. Michael Pecht, my advisor, for his support and guidance throughout my academic endeavor.

I wish to thank Dr. Abhijit Dasgupta and Dr. Donald Barker for attending my presentations, reviewing my research plans, and providing so many valuable suggestions. I am also very grateful to Dr. Diganta Das for his constant support.

I appreciate all of the technical reviews, critique, and suggestions that were provided by the CALCE team members, in particular, Vidyu Challa, Sony Mathew, Dr. Hao Yu, Weiquiang Wang, and Shunfeng Cheng.

Many thanks to Dr. David McElfresh and Dr. Kenny Gross from Sun Microsystems for the extensive discussions, suggestions, and technical reviews. Also thanks to Roger Blythe and Dr. Kalyan Vaidyanathan for the Sun Fire™ hardware and software support. I am also grateful for Myra Torres' review of my technical presentations and for her suggestions on how to improve my work.

Special thanks to Dr. Roland Timsit, from Timron Advanced Connector Technologies, for his invaluable training on electrical contacts.

Table of Contents

List of Tables

List of Figures

Chapter 1: Reliability of IC Sockets

1.0 Introduction

Enterprise servers are utilized by many corporations around the world to handle critical software applications and data. Web portal transactions, video and music storage, bank account management, corporate payrolls, and databases are just a few examples. IC sockets in these enterprise servers are expected to provide the highest levels of quality and reliability, because failure in this application environment results in a significant loss of revenue for the customer. There are three IC socket contact technologies that are typically used in industry: CIN::APSE (fuzz button), stamped metal, and elastomer. Elastomer sockets in general are used because they provide a low cost alternative and because they can be easily adapted to practically any customer package design. However, the reliability of the elastomer contact in server applications is not well understood. This dissertation provides a comprehensive study of the resistance behavior of elastomer contacts, and develops models for the estimation of contact reliability in an enterprise server application.

1.1 Motivation for Research

While many studies have been performed to analyze the properties and behavior of the elastomer contact, there is practically no information about the actual operating conditions at the contact interface and the long term behavior of the contact under mechanical loads. Furthermore, there is no experimental data to define PoF

models that would allow the estimation of contact reliability in production representative assemblies.

1.2 Objectives of Thesis

The main objective of this research is to define the reliability of an elastomer contact that operates in a high-end server application. To achieve this goal the following secondary objectives were defined: i) Identify the operating environment of the IC socket contact; ii) Define a methodology for the detection of contact resistance degradation; iii) Investigate the long term resistance behavior of contacts under mechanical load; iv) Define a PoF model for the contact resistance of elastomer sockets; v) Define the reliability of the elastomer contact in a server application.

1.3 Overview of Thesis

Quality, reliability, health monitoring, and electronic prognostic applications, can not be successfully developed and deployed without a clear understanding of the operating environment of the component under analysis. In Chapter 2 the temperature and relative humidity environment for an IC socket in a high-end server application is outlined. The experimental setup is presented, where a network of sensors and health monitoring tools are utilized to determine operating profiles for the server, motherboard, LGA package, IC, and socket contact interface. The relationship between microprocessor junction temperature and contact temperature and humidity are discussed. Temperature changes across the socket assembly are provided as a function of microprocessor activity.

Chapter 3 presents a novel approach for the modeling and monitoring of contact resistance. The technique is introduced for reliability and health monitoring applications. A model for the true contact area radius as a function of temperature is discussed. A model for the elastomer contact resistance is presented. The approach is demonstrated for the estimation of contact resistance during a temperature cycle experiment. The methodology steps and implementation are outlined.

Chapter 4 presents a study on the contact resistance behavior of elastomer sockets as a function of time and temperature. A model for the mean a-spot radius as a function of time is presented, and a model for the contact resistance is discussed. The implementation of a log-normal-PoF model to estimate contact resistance during the first year of operation is outlined. Chapter 5 discusses the effects of electrical bias on elastomer contacts.

Chapter 6 outlines potential sources of failure in IC socket assemblies. The differences between two contact design alternatives are described from the reliability point of view. Other sources of failure presented include manufacturing, system assembly, system storage and transportation, system operation, and system service and repair. The contributions from this research, as well as suggested future work, are provided in Chapter 7.

Chapter 2: Assessing the Operating Temperature and Relative Humidity Environment of IC Sockets in Enterprise Servers

2.0 Introduction

Microprocessors in high-end computer systems are typically connected to printed circuit boards (PCB) by either solder joints or by IC sockets. IC sockets are used as an alternative to solder joints because they can provide a repairable, heatless, high density, and reliable interconnect solution. In some applications these sockets provide interconnection for over 32000 power, ground, and signal lines in a single server.

Current industry practices, such as ANSI/EIA-364 and Telcordia GR-1217-CORE, for the evaluation of IC sockets rely on the execution of predetermined stress loads (e.g., temperature, humidity, shock, vibration), at predetermined load intensities without consideration to the operating conditions, IC socket characteristics, or reliability requirements [1]-[3]. Similar methods are used for the evaluation of test and burn-in sockets [4]. The qualification of IC sockets under current practices does not supply the information needed to derive acceptable reliability models and operating life estimates [5]. To assure high levels of reliability for the IC socket it is necessary to perform tests that mimic the actual component operating environment, providing acceleration of relevant failure mechanisms.

Over the socket life cycle, dust, shock, vibration, temperature, temperature cycling, humidity, and corrosive gas exposure, can trigger failure mechanisms such as creep, stress relaxation, contact wear, stiction, deformation, and corrosion among others, which can result in permanent or intermittent contact resistance changes [6], [7]. For IC sockets, temperature and humidity environmental stresses are important drivers of failure [6]. Understanding these operating conditions, and the behavior of the IC socket over time, is paramount for socket reliability and prognostic analysis. Health Monitoring (HM) and Electronic Prognostics (EP) are methods of gathering and analyzing information about a component or system during actual application conditions, and allow the derivation of reliability models and life estimates [8].

This study evaluates the operating temperature and relative humidity environment of an IC socket inside of an enterprise server, enabling quality, reliability, and prognostic analyses. These parameters are monitored over three months of normal operation. Variations during power-on transitions are characterized. Microprocessor activity and its effect on the IC socket environment are analyzed. Thermal profiles of the silicon die, microprocessor package, printed circuit board (PCB), and data center are identified.

2.1 Contact Resistance Distribution

An IC socket is an electro-mechanical system that, by means of compression, provides a separable, repairable, and solderless electrical interface between an IC component and a PCB [6]. The IC socket is composed of a polymer housing (for handling, physical protection, electrical isolation, load bearing and alignment), and an

array of contacts. Three common IC socket contact technologies are stamped metal, fuzz button, and metal-filled elastomer. For the experiment described in this publication Tyco 1.0 sockets were utilized. The Tyco socket is a 37 x 37 array of silver-filled elastomer contacts that are molded onto a Kapton polyimide film and attached to a thermoplastic housing. The socket dimensions are 55.0x57.0x3.3 mm, excluding two alignment posts, as shown in Figure 1 (see Appendix I).

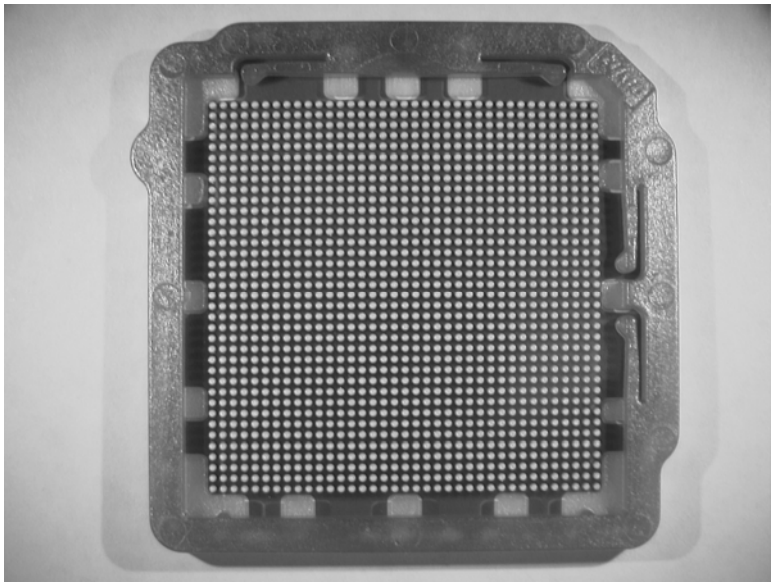

Figure 1. Tyco 1.0 elastomer socket used for the experiment. This design has 1369 contacts arranged in a 37x37 array. The socket is 55mm wide and 57mm long

When the IC socket contacts are compressed between an IC package and a PCB, the silver particles inside the elastomer matrix touch each other, creating a percolation network, as illustrated in Figure 2. An important characteristic of this technology is that all metal-to-metal contacts that are created with the applied compressive load are encapsulated by the elastomer, limiting the exposure to contaminants and humidity in the air. A detailed analysis of the compressive load and load distribution of IC socket assemblies is provided in [9] and [10].

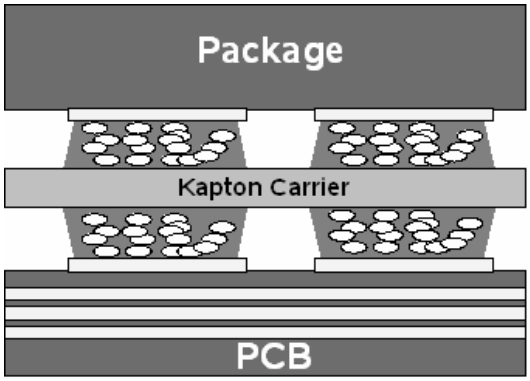

Figure 2. Cross-sectional illustration of an elastomer socket assembly with applied compressive load. The silver particles in the elastomer matrix contact each other and create a percolation network

2.2 Health Monitoring and Electronic Prognostics

Health Monitoring and Electronic Prognostics methods consist of the continuous assessment of a product's operating environment and performance, to enable the derivation of reliability models, estimates of remaining life, and detection of deviations from expected normal operating conditions. These methods are typically implemented in mission-critical or safety-critical systems such as aircraft, nuclear power plants, medical equipment, military applications, and enterprise servers. HM can be performed by means of diagnostic, prognostic, or life consumption monitors. Diagnostic monitors determine the current state of health of a system, identifying potential problems. Prognostic monitors analyze system health information, estimating future reliability based on the physics of failure (PoF). Consumption monitors measure the operating conditions and assess accumulated damage, providing estimates of remaining life [11].

The following sections demonstrate a setup for HM of an IC socket's operating environment and the collection of information. The substantial data that is

acquired in this manner enables the identification of key failure mechanisms, the development of accurate reliability models and quantitative qualification plans, and the overall implementation of EP tools.

2.3 Experimental Setup

A Sun Fire™ 6800 server was used as the test vehicle to assess the operating environment of the elastomer socket described in section 2.1. This enterprise server has six motherboards, each one with four UltraSPARC© III microprocessors, cache memory, DIMM, and a variety of active and passive components. The IC sockets and microprocessors were installed above the PCB, compressing the contacts to specification (60-80 g each) by means of a heatsink, bolster plate, springs, and screws, reducing the average contact height from 940 μm down to 650 μm. The microprocessor assembly is illustrated in Figure 3.

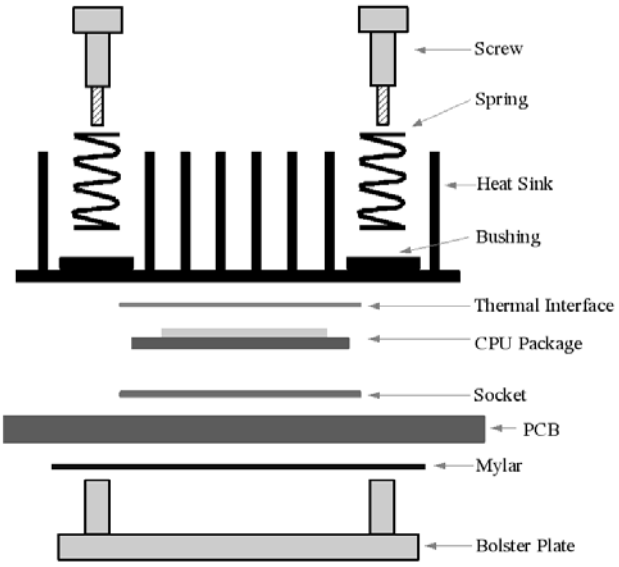

Figure 3. Illustration of a microprocessor assembly used to provide compressive loads for the elastomer socket. The thermal interface and insulating Mylar layers are shown

Due to assembly space constraints it was necessary to make two modifications to the socket housing that would allow the installation of sensors at the contact interface. First, a small perforation was made to embed a thermocouple for the monitoring of air temperature. Second, a cavity was made to embed a modified Honeywell HIH-3610-004 relative humidity sensor. The sensor plastic housing was cut and polished to a size of 6x4x1.5mm and fitted to this cavity. None of these modifications compromised the structural integrity of the housing or contact alignment.

Thermocouples were installed on the top surface of the microprocessor packages and on PCB locations near the IC socket. HOBO® U10-003 data recorders were attached to the server chassis to monitor the temperature and relative humidity of the data center. One recorder was placed near the floor level (lower recorder) and another near the system air intake (upper recorder), next to the motherboards. Overall 10 IC sockets, 10 microprocessors, and 3 PCBs were wired, providing 23 thermocouples, 3 internal relative humidity sensors, and 2 external temperature and relative humidity sensors.

The Continuous System Telemetry Harness (CSTH), part of the Sun Fire™ server, was used to monitor the junction temperature of all 24 microprocessors. The CSTH manages a sensor network, allowing the capture, conditioning, synchronizing, and storage of telemetry signals for later use by HM and EP applications [13].

An Agilent E3643A DC power supply was used to power the humidity sensors and a HP 34970A data acquisition/switch was used to measure the

thermocouple and humidity sensor outputs. Both instruments were controlled by means of a computer, a GPIB (IEEE 488) interface card, and a C-language program. The temperature and humidity sensors were monitored at five-minute intervals. The microprocessor temperature was monitored at one-minute intervals. The setup for the microprocessor assembly and server are illustrated in Figures 4 and 5.

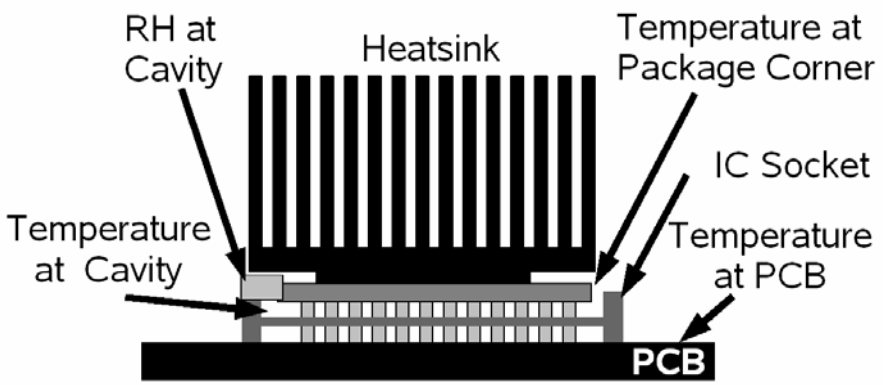

Figure 4. Illustration of sensors installed on the microprocessor assembly. Thermocouples are placed on the socket, package and PCB. A relative humidity sensor is placed in the socket housing, above the Kapton carrier. Bolster plate, springs, screws, and other assembly components not shown for clarity

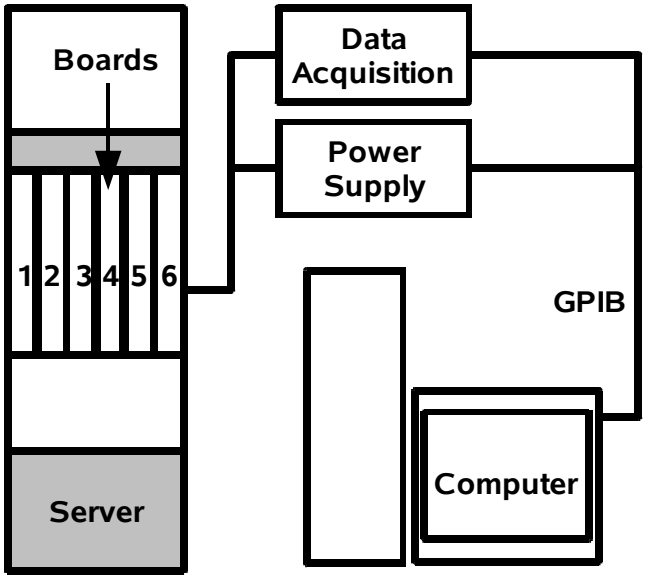

Figure 5. Illustration of the server setup with data acquisition, power supply, and signal monitoring for IC sockets. The CSTH functions are integrated into the server and not shown

The sensor network and the CSTH were tested and calibrated over a three-day period with power-on and power-off conditions. The temperature and relative humidity of the air entering the system, while the motherboard power was off (system fans on), were compared with measurements from sensors at the IC socket contact interface. When the sensor and system calibration was completed the experiment was initiated. The microprocessor executed a Linpack-based script with two-hour cycles (one hour idle, one hour running the benchmark test), simulating server demand during operation. The experiment was carried out for three months inside a data center located in San Diego, CA.

2.4 Experimental Results

2.4.1 Temperature and Relative Humidity Profile for Power-on Transitions

The first activity in this experiment was the monitor of temperature and relative humidity during power-on transitions. With the motherboards powered-off and the cooling fans operating to provide airflow, the temperature and relative humidity at the socket interface was allowed to stabilize and match those of the data center, as indicated by the HOBO® recorders. After four hours all motherboards were powered-on, initializing the operating system and test script for each microprocessor. The effects of this power-on transition on the operating environment of the IC socket are shown in Figure 6.

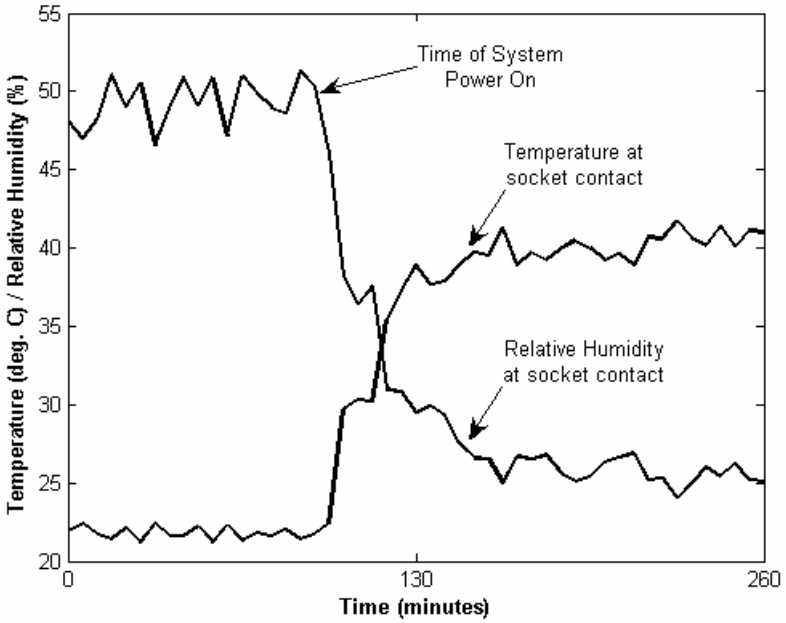

Figure 6. Average temperature and relative humidity profile of the IC socket contact interface in a power-on transition

As the microprocessor junction temperature increased, the relative humidity at the socket interface decreased significantly, from a 49%RH average (45-52% range) down to 24%RH (22-28% range), all in the course of one hour. In the same period of time the air temperature at the socket interface increased from a 22 °C average (21-23 °C range) up to 41 °C (38-45 °C range). Evaluations performed for automotive assemblies have measured similar shifts in temperature and relative humidity inside enclosed connectors [14].

An important observation from this data is the change in temperature and relative humidity ranges after the system power is turned on. When the microprocessor temperature stabilizes, relative humidity readings at the socket contact interface are more stable, changing only by 2-3% on any given signal. The same is true for the air temperature, which shows less than 3 °C variation over time.

In the experiment it was also observed that three temperature measurements were consistently higher than other measurements. These signals were found to be monitoring microprocessors on motherboards at the edge of the system, next to the chassis (labeled as 1 and 6 in Figure 5).

While an increase in temperature and a reduction in relative humidity are expected inside electronic assemblies in normal operation, the magnitude of change and correlations with external environmental variables were unknown for the IC socket contact interface. For some IC socket technologies, such as those that utilize stamped metal contacts, temperature and humidity are key drivers of corrosion and fretting mechanisms [15]. Having accurate information about the actual operating environment allows better and more realistic reliability evaluations and enables EP implementations [16], [17].

2.4.2 Temperature Profile of Microprocessor Assembly During Server Operation

The temperature profile of three microprocessors over a ten-hour period is shown in Figure 7. Each one of the temperature signals cycled every two hours. The lower temperatures were reached when the microprocessor was idle. The higher temperatures were reached when the microprocessor was executing benchmark tests. The observed variability at each one of the temperature levels was caused by low resolution sensors in the microprocessor, which can only detect changes greater than 1 °C. The recorded temperatures of the microprocessor die, microprocessor packages, socket contact (air), and PCBs are summarized in Table 1.

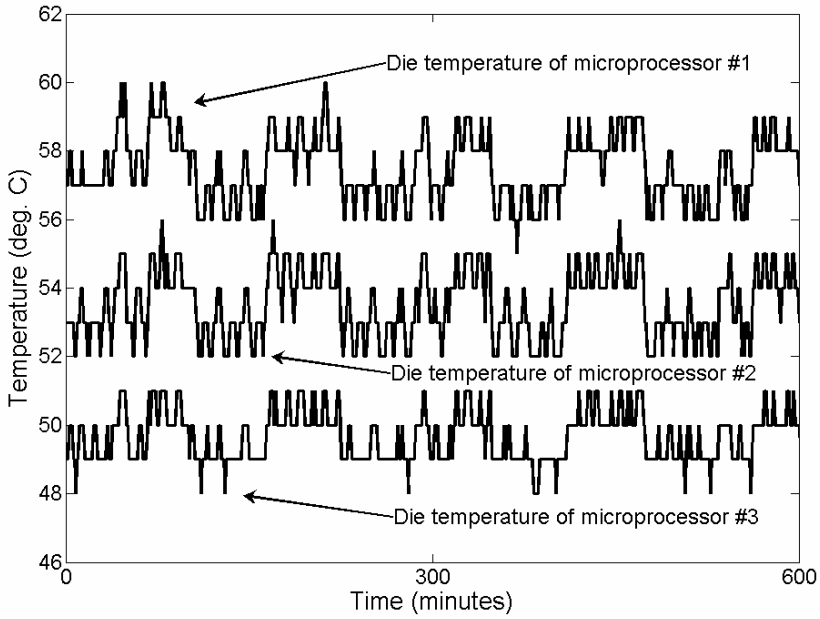

Figure 7. Temperature signals of three microprocessors monitored by the CSTH during a ten-hour period. The higher temperatures result from microprocessor running benchmark testing while the lower temperatures result from microprocessor idle state

Table 1. Recorded temperatures during the experiment

Sensor Location	Sample Size	Temperature, Idle CPU (°C)	Temperature, Active CPU (°C)
Die	24	52.5 (48.0-58.0)	53.9 (48.0-60.0)
Package	10	42.4 (39.4-47.7)	43.4 (39.4-49.0)
Socket Contact	10	41.0 (38.3-45.3)	42.0 (38.6-46.4)
PCB	3	37.0 (35.9-38.7)	37.8 (36.0-39.2)

Overall the average temperature changes (deltas) during operation were1.4 °C, at microprocessor die, 1.0 °C, at microprocessor package, 0.9 °C, at IC socket contact (air), and 0.8 °C at the PCB. These results indicate that reliability evaluations of this component (in this system) can require a smaller number of temperature cycles to accelerate relevant failure mechanisms, when compared to those specified by industry standards (typically above 1000) [1], [2]. For the same reasons it can be concluded

that accelerated temperature storage tests can be more effective in simulating normal operating conditions for this application. The microprocessor, package, socket, and PCB temperature signals could be used by EP tools to detect thermal anomalies and to estimate stresses in the assembly induced by temperature gradients and temperature cycling. Tools such as the Multivariate State Estimation Technique (MSET) and Sequential Probability Ratio Test (SPRT) can be used to detect the incipience of failures, aid in the identification of root causes of failure, and reduce No Trouble Found (NTF) events [11], [12].

2.4.3 Relative Humidity Profile Induced by Microprocessor

The temperature and relative humidity measured at the IC socket interface for a ten-hour period is shown in Figure 8. The temperature, represented by the signals at the top of the figure, was on average 41.0 °C (38.3 to 45.3 range) when the microprocessor was idle and 43.4 °C (39.4 to 49.0 range) when the microprocessor was executing benchmark tests. Under the same conditions the relative humidity, represented by the signals at the bottom of Figure 8, was on average 24.0% (21.7 to 27.3% range, idle) and 23.3% (20.8 to 27.3% range, running benchmark tests). The cyclic changes in socket ambient temperature result in less than 3% variation in the relative humidity. For the samples monitored, and within the temperature range considered for this study, a 0.8% reduction in relative humidity can be expected for every 1 °C increase in temperature. The relative humidity and temperature monitor data, as illustrated in Figure 8, could be used by EP tools to estimate corrosion rates of metal connectors, degradation of materials over time, and occurrence of temperature and humidity accelerated events.

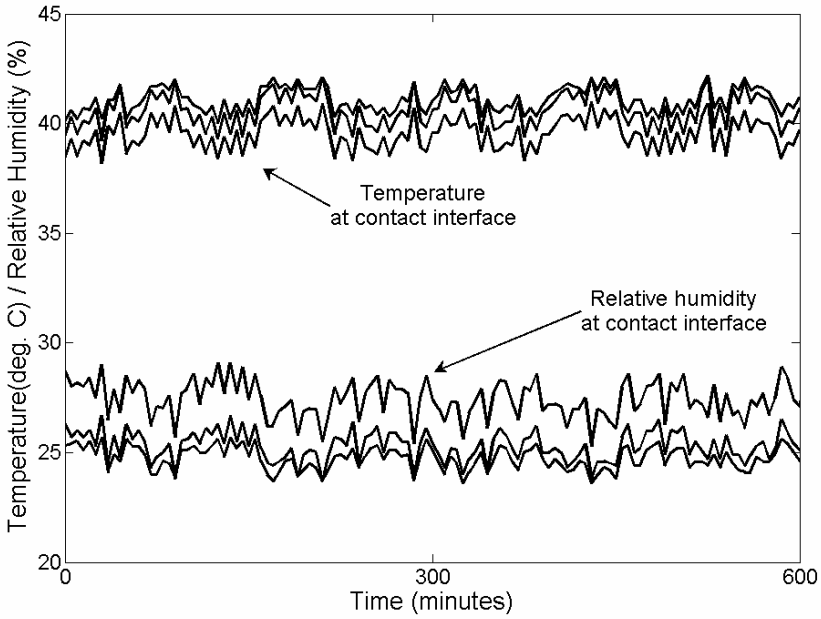

Figure 8. The temperature (°C, represented by the upper signals) and relative humidity (%, represented by the lower signals) at the IC socket interface for a ten-hour period are shown. Corresponding microprocessor temperatures for the same period are shown in Figure 7

2.4.4 Temperature and Relative Humidity Profile of the Data Center

The temperature and relative humidity of the data center environment for a two-month period is illustrated in Figure 9. The temperature was 21.6 °C average (20.4-24.4 °C) with relative humidity at 45.6% average (32.2-54.1%). The measured temperatures were consistent with those expected of computer rooms but the relative humidity was at times above the suggested range of 45-55% [18].

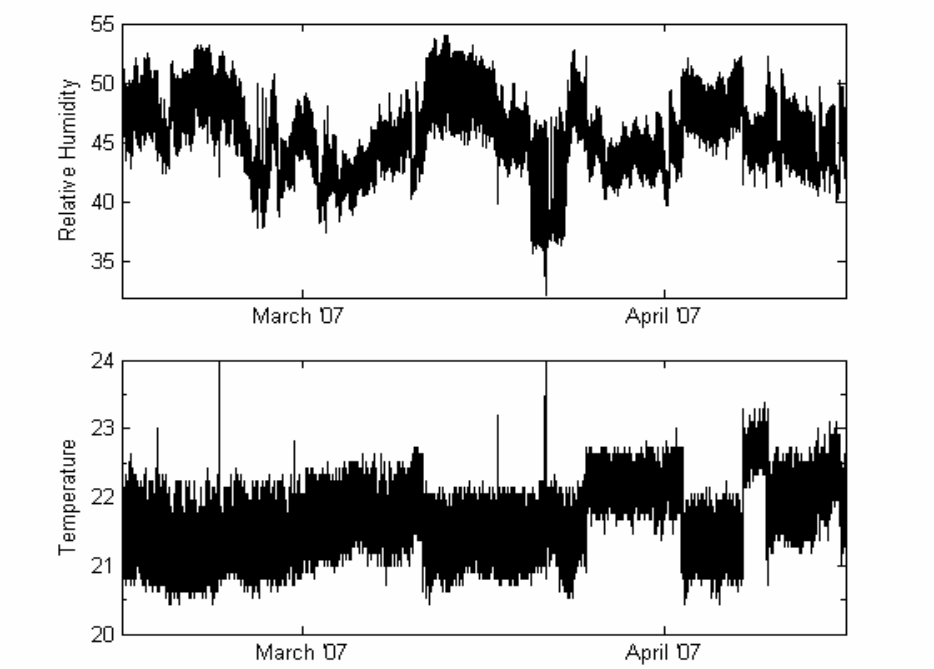

Figure 9. Temperature (ºC) and RH (%) in data center in a two-month period

These results were obtained with the HOBO® recorder located next to the motherboards (upper recorder). Similar measurements were obtained with the recorder located near the floor level (lower recorder). Temperatures at the upper recorder were found to be on average 1 °C higher and relative humidity 3% lower than those obtained by the lower recorder. These differences are caused by the heat generated by the servers in the data center.

2.5 Conclusions

In this paper the temperature and relative humidity environment of an IC socket inside an enterprise server was evaluated. The environment, at the socket contact interface, was characterized during power-on transitions and monitored during normal operating conditions. The temperature of the microprocessor die, packages, PCBs, and data center were measured for the duration of the test. The

relative humidity in the data center was also monitored. The microprocessor die temperature was found to be on the average 53 °C (48-60 °C range), which resulted in 41 °C and 23% relative humidity at the contact interface. The variation in temperature and relative humidity during operation was found to be less than 3 °C and 3% respectively. For the temperature range considered in this experiment, and for this server application, the relative humidity can be expected to decrease 0.8% for every 1 °C increase in temperature. The relative humidity at the IC socket interface was found to be 25-30% lower than that of the data center environment. The data suggests that, for this particular server application, temperature storage tests can be optimal toward accelerating the non-bias operating environment of the socket. In addition, given the relatively benign temperature cycle profile, short temperature cycle evaluations (<1000 cycles) should be considered to simulate power cycle, temperature cycle, and interconnect aging.

The temperature and relative humidity profiles identified in this experiment can be used with physics of failure models to assess the interconnect reliability, to determine what failure mechanisms are relevant for the operating environment, to estimate accumulated damage as a function of time, to establish correlations between environment and interconnect behavior, and to train prognostic models for the detection of precursors of failure. Experiments and models that are based in industry standards such as ANSI/EIA-364 and Telcordia GR-1217-CORE, can not provide this information, lacking insight into the physics of failure of the component and the operating environment.

Chapter 3: Modeling of IC Socket Contact Resistance for Reliability and Health Monitoring Applications

3.0 Introduction

In enterprise servers, Integrated Circuit (IC) sockets are used to interconnect Land Grid Array (LGA) packages with Printed Circuit Boards (PCB) [12]. These interconnect systems provide many manufacturing and reliability advantages over traditional solder joints, particularly for high density applications where tens of thousands of power, ground, and signal lines are required in a single system. Reworkability, low cost, and maintainability are some other benefits of this technology [6], [19]-[21].

When evaluating IC socket reliability, stress environments are applied to induce the occurrence of failure mechanisms, resulting in either permanent, or intermittent resistance events (failure or degradation) [6], [7]. For reliability evaluations, these test conditions are typically based on industry standards (such as ANSI/EIA-364, and Telcordia GR-1217-CORE), and require the monitoring of test devices, called daisy chains, during Temperature Cycle (TC), High Temperature Storage (HTS), Temperature Humidity Bias (THB), and Mixed Flowing Gas (MFG) tests [1], [2]. In health monitoring applications, the resistance of one or more test contacts, called canary devices, is monitored while the system is being subjected to typical operating loads, and compared to an initial reference value [22], [23]. When the monitored resistance is determined to exceed the specification threshold, the

device is considered a failure [1], [24]. Similar procedures are used for the evaluation of solder joint reliability [25]. However, this approach does not consider the physics of failure (PoF) of the contact [26], the contact behavior in the stress environment, or the stress level variability during typical operating conditions. Furthermore, the use of threshold values for the detection of changes in resistance results in decreases of sensitivity, and increases the probability of false alarms and missed alarms. When the threshold is placed too close to the monitored signal, frequent false alarms are triggered. When the threshold is placed too far from the monitored signal, true alarms go undetected.

This paper describes a methodology for the modeling and monitoring of contact resistance in electrical interconnects, called M-SPRT (Maxima-SPRT). In this approach, a physics of failure model is used to estimate the maximum expected resistance as a function of temperature, and a Sequential Probability Ratio Test (SPRT) is used to detect changes in resistance behavior.

3.1 Introduction to the Sequential Probability Ratio Test

The SPRT was used in this methodology for the detection of changes in electrical resistance. In SPRT, the residual (Δ_R), between a resistance measurement (R_m), and a resistance estimate (R_e), is evaluated against a null (H_0), and alternative (H_1) hypothesis. The hypotheses are statements that define the statistical distribution, and distribution parameters that are considered healthy versus degraded for the device under test [11]. For a series of resistance residuals between measurements and

estimates Δ_{R1}, $\Delta_{R2}\ldots\Delta_{Rn}$, the probabilities of occurrence of the alternative, and null hypotheses are respectively given by

$$f(\Delta_{R1})f(\Delta_{R2})...f(\Delta_{Rn}) = F(\Delta_R) \tag{3.1}$$

$$g(\Delta_{R1})g(\Delta_{R2})...g(\Delta_{Rn}) = G(\Delta_R) \tag{3.2}$$

The probability ratio $F(\Delta_R)/G(\Delta_R)$, evaluated against accept (B) and reject (A) limits, is represented by

$$B < \frac{F(\Delta_R)}{G(\Delta_R)} < A \tag{3.3}$$

The evaluation of (3.3) can result in three different outcomes, which are illustrated in Figure 10. If the probability ratio is equal to or greater than limit A, then there is strong statistical evidence that the sequential residuals Δ_{R1}, $\Delta_{R2}\ldots\Delta_{Rn}$ exhibit degraded behavior (hypothesis H_1) [27]. If the probability ratio is equal to or smaller than limit B, then there is no evidence that the observations are degraded (data are consistent with healthy behavior hypothesis, H_0). If the ratio $F(\Delta_R)/G(\Delta_R)$ is between the limits A and B, then more observations are required to define the state of the device under test.

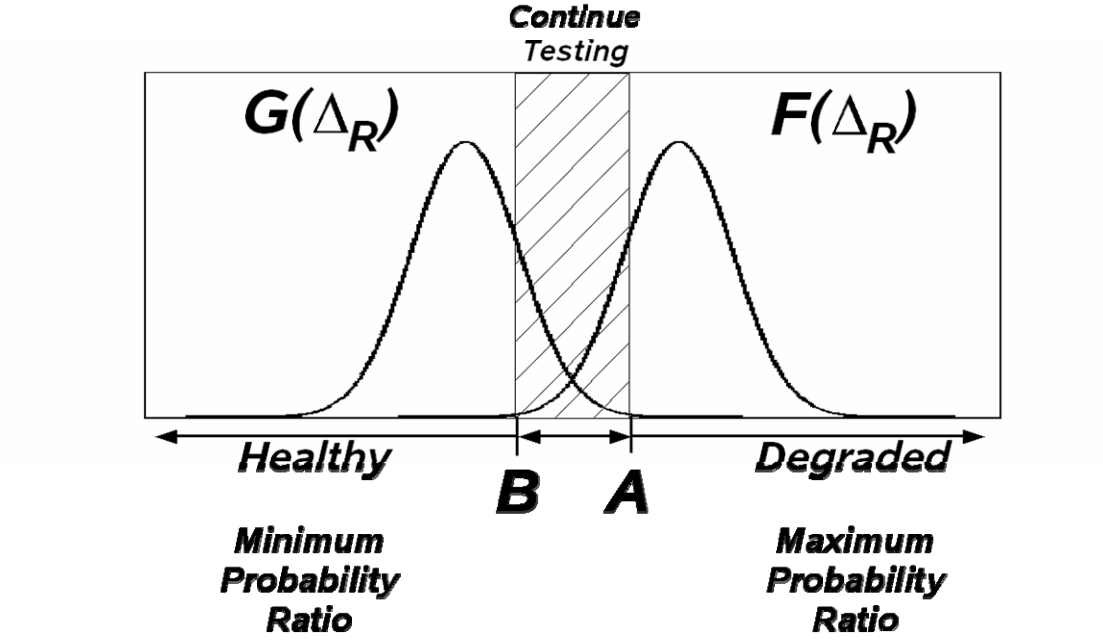

Figure 10. Potential outcomes in the evaluation of the probability ratio

The limits *A,* and *B* are respectively defined as functions of the false alarm, and missed alarm probabilities α, and β. Therefore, in the evaluation of a null, and alternative hypothesis, it is possible to have either of four outcomes:

- Reject H_0 when H_0 is true, with probability α (Known as type I error).
- Reject H_0 when H_1 is true, with probability 1-β (correct decision).
- Accept H_0 when H_1 is true, with probability β (Known as type II error).
- Accept H_0 when H_0 is true, with probability 1-α (correct decision).

With these considerations, the limits *A,* and *B* are defined as

$$A = \frac{1-\beta}{\alpha} \tag{3.4}$$

$$B = \frac{\beta}{1-\alpha} \tag{3.5}$$

If the resistance residuals at a given temperature are assumed to vary only as a result of random events (e.g. measuring error, system variability, sensor variability), then it is reasonable to assume that the residuals would be normally distributed around a mean value. The hypotheses, assuming a normal distribution of residuals, can be expressed as follows.

- Null H_0: The mean of the resistance residuals (Δ_{Ri}) is μ_0=0, with standard deviation σ.
- Alternative H_1: The mean of the resistance residuals is μ_1, with standard deviation σ.

The probability distributions for $F(\Delta_R)$, and $G(\Delta_R)$ (H_1, and H_0) are given by

$$F(\Delta_R) = \frac{1}{(2\pi)^{n/2}} e^{-\frac{1}{2}\sum_{i=1}^{n}\left(\Delta_{Ri}-\mu_1\right)^2} \tag{3.6}$$

$$G(\Delta_R) = \frac{1}{(2\pi)^{n/2}} e^{-\frac{1}{2}\sum_{i=1}^{n}\left(\Delta_{Ri}-\mu_0\right)^2} \tag{3.7}$$

Inserting (3.4), (3.5), (3.6), and (3.7) into (3.3), setting μ_0=0, and simplifying the inequality, resulted in test criteria (SPRT index) for the resistance measurements:

$$Ln\left(\frac{\beta}{1-\alpha}\right) < \frac{\mu_1}{\sigma^2}\sum_{i=1}^{n}\left(\Delta_{Ri} - \frac{\mu_1}{2}\right) < Ln\left(\frac{1-\beta}{\alpha}\right) \tag{3.8}$$

where μ_t is the mean defined by alternative Hypothesis, σ is the standard deviation for H_0 and H_1, and $\underline{\Delta_{Ri}}$ is the sequential residual *i*.

3.2 Methodology

The M-SPRT methodology consists of five steps: resistance characterization, physics of failure model selection, model validation, SPRT definition and training, and resistance monitor. The methodology is illustrated in Figure 11.

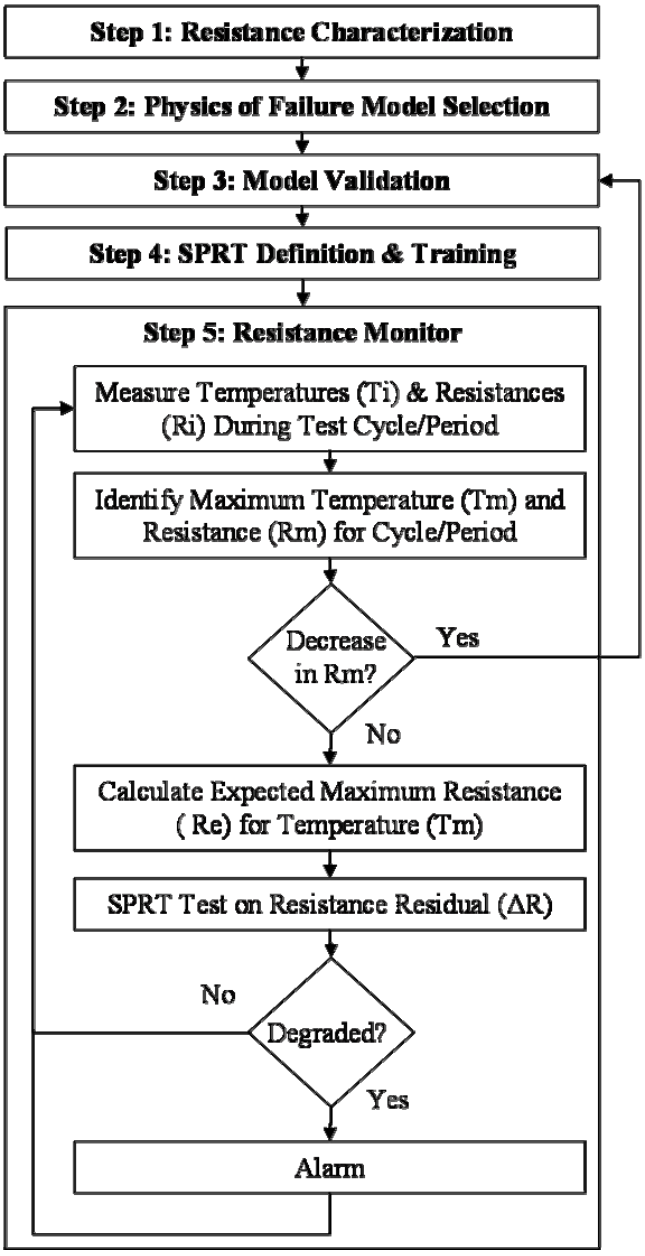

Figure 11. The M-SPRT methodology for monitoring contact resistance of electrical interconnects

3.2.1 Resistance Characterization

When the methodology is considered for a reliability application, the characterization may be performed using daisy chain packages, and a test assembly. When the methodology is considered for a health monitoring application, the characterization may be performed with a system assembly, and canary devices.

The resistance behavior of the electrical interconnect (contact) is analyzed as a function of temperature (T). Resistance measurements are performed starting at 25 ºC (room temperature), and in 10 °C increments, up to the maximum expected temperature of the contact during the evaluation. As an alternative, the maximum recommended operating temperature of the contact (as indicated in the specification) can be used as the upper limit in the characterization test. For each test condition, the resistance is measured when the assembly and contacts reach the target temperature. The resistance characterization provides the expected (healthy) behavior of the contact as a function of temperature.

3.2.2 Physics of Failure Model Selection

The contact design, materials, mechanical load assembly, environmental conditions, and fundamental contact theory are analyzed to explain the resistance behavior that was observed during the characterization experiment. A PoF model is selected to estimate the contact resistance as a function of the stress environment. Parameters for the model are extracted from the characterization data using regression analysis. Finally, the PoF model is tested against the characterization data, and the measuring error levels are verified to be within an acceptable range (e.g. estimate error <0.5 mΩ).

3.2.3 Model Validation

The model validation is performed with the test assembly that was used during the resistance characterization. For a reliability application, the assembly is subjected to stress levels that are representative of the intended test environment. For health monitoring applications, the assembly is subjected to nominal operating conditions. The temperature (T_i) and resistance (R_i) are monitored continuously, identifying the maximum temperature, and maximum resistance (R_m) of each test cycle/period. When the experiment is completed, maximum resistance estimates (R_e) are generated for each one of the maximum temperatures using the PoF model. The estimates are compared to the measurements, and the model is calibrated accordingly. This model calibration is repeated until the resistance residual (the difference between estimated and monitored maximum resistance) is acceptable (e.g. Δ_R<1mΩ).

3.2.4 SPRT Definition and Training

The SPRT definition and training are performed with measurements that are representative of the test or system environment. The measurements are performed until a sufficient number of test cycles or hours are accumulated, enough to provide a complete view of the application environment (either accelerated test, or health monitoring). During the training period, the maximum temperature, and the resistance of each test cycle or operating period are obtained from measurements (T_i, R_i); and a resistance estimate (R_e), and residual (Δ_R) are calculated. The resulting array of residuals is used to calculate the mean, and standard deviation of the null hypothesis (H_0). If the model is accurate, and if the maximum test conditions are consistent during the training period, the mean of the residuals would be found to be zero (for a

normal distribution assumption). The mean μ_1 of the alternative hypothesis (H_1) is selected considering the null hypothesis mean, and standard deviation (e.g. $\mu_1 = \mu_0 + 3\sigma$, $\sigma_1 = \sigma_0$). Finally, the false alarm, and missed alarm probabilities (α, β) are selected, and the SPRT index of (3.8) is defined.

3.2.5 Resistance Monitor

The resistance and temperature of the test samples are continuously monitored for the duration of the experiment (the test duration for a reliability evaluation, or the product life for a health monitoring application). The maximum contact resistance and temperature values are extracted for each test cycle or period, the expected resistances are calculated with the PoF model, and the resistance residuals are tested with the SPRT. If any residual is found to be statistically different than that expected by the null hypothesis, then the maximum contact resistance is considered degraded, and an alarm is raised. If the residual is not found to be different, then the maximum contact resistance is considered "healthy." After either case, the monitoring process continues. If during the evaluation the resistance measurements are found to decrease over time, then the model validation, and the SPRT definition and training are repeated, setting new values for the null and alternative hypotheses, and updating the SPRT index (3.8). This retraining improves the test sensitivity by considering situations where the contact resistance improves after initial assembly. The resistance monitor process for a reliability application (temperature cycle test) is illustrated in Figure 12.

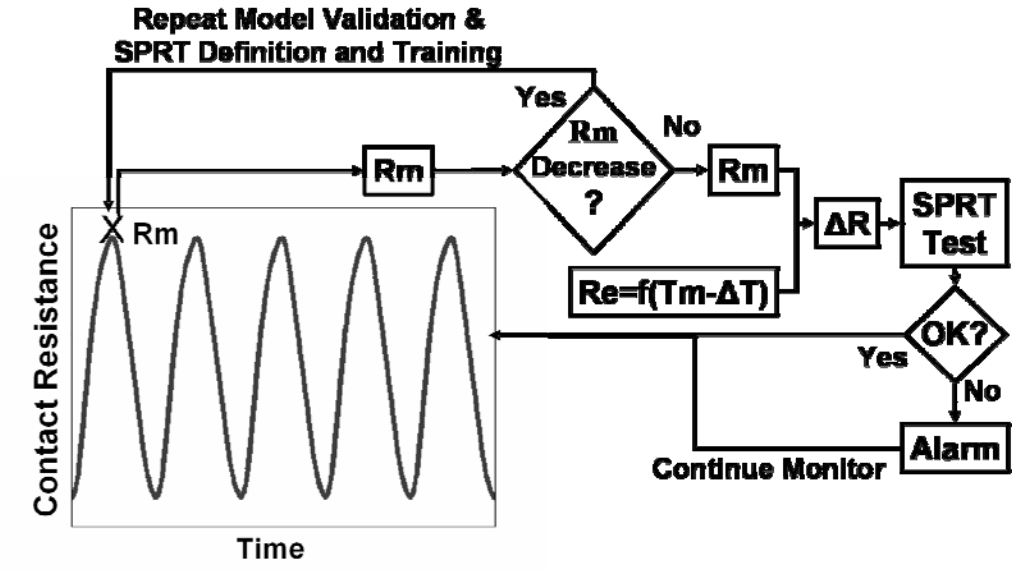

Figure 12. Process for the monitoring and analysis of contact resistance data during a temperature cycle test. Rm is the maximum resistance during a test cycle

3.3 Experimental Demonstration

The M-SPRT methodology was demonstrated for a reliability evaluation, using daisy chain packages as test vehicles, and a temperature cycle test as the stress environment. The implementation of the methodology for health monitoring applications would follow the same approach, but measuring canary devices during typical system operation.

3.3.1 Experimental Setup

The IC socket utilized for the experiment is a 37 x 37 full array of Ag-filled elastomer contacts. The contacts are molded into a Kapton film carrier, and protected by a thermoplastic housing. The test assembly, which provided mechanical load and access for resistance monitoring, consisted of a heatsink, daisy package, test board, bolster plate, insulating Mylar, TIM, springs, screws, and IC socket [9]. When under

mechanical load, the IC socket and test assembly create the circuit illustrated in Figure 13. To monitor the socket resistance during the experiment, a Keithley 7001 switch, and 580 microOhm meter were used.

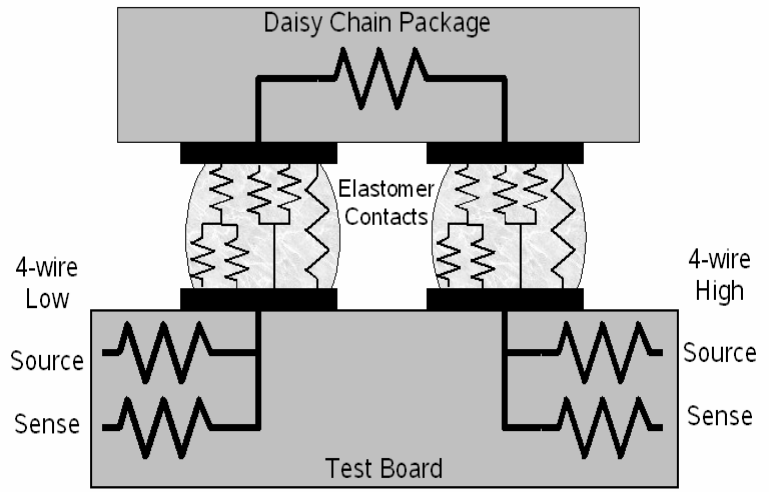

Figure 13. Illustration of the daisy chain created by the test assembly and elastomer socket under compression. The interconnect matrix created by the Ag particles in the elastomer are represented by the resistive network inside the two contacts

As shown in Figure 13, the total resistance consisted of circuit resistance (test board + daisy chain), bulk contact resistance (two contacts in series), and contact to pad resistances. Contact to pad resistance (Au to Ag) is very small in relation to bulk and circuit resistances, so was ignored. The circuit resistance was found to be on average 16.7 mΩ. The resistance of an individual elastomer contact, from test assembly measurements, was estimated by

$$R_i = \frac{R_t - 16.7}{2} \tag{3.9}$$

where R_t is the total circuit resistance (board and package resistance, plus 2 contacts in series). The measuring system error for the test setup was measured, and found to be <0.05 mΩ.

3.3.2 Resistance Characterization

The resistance behavior of ten daisy chains was evaluated at six temperature conditions: 25, 35, 45, 55, 65, and 75 °C. For each condition, the test assemblies were allowed to dwell from 30 to 60 minutes, until the temperature and resistance measurements were stable. For each temperature setting, the resistance of individual contacts was estimated with (3.9), then recorded, finding resistance mean values of 4.8 mΩ at 25 °C, and 7.5 mΩ at 75 °C, as shown in Table 2.

Table 2. Resistance values from characterization test

Temperature (°C)	Mean (mΩ)
25	4.8
35	5.4
45	5.9
55	6.5
65	7.0
75	7.5

3.3.3 Physics of Failure Model Selection

The increase in elastomer contact resistance as a function of temperature resulted from the interaction between the Ag particles and the elastomer. As the temperature was increased, the elastomer expanded, disrupting the Ag-Ag contact matrix inside the elastomer. The thermal expansion decreased the effective a-spot

area of the contact, and increased the overall resistance [28]-[35]. The contact resistance, as a function of the effective a-spot radius, resistivity of Ag, and applied temperature, can be described by [15], [36]

$$R_e = \frac{\rho_T}{2a} \tag{3.10}$$

$$\rho_T = \rho_{20} + \rho_{20} * (T - 293.15) * 0.0038 \tag{3.11}$$

where the constant 0.0038 is the thermal coefficient of resistivity for Ag.

Values of resistivity (ρ_T), and a-spot radius (a) were estimated for each test sample and temperature, using the monitored resistance, and (3.10) and (3.11). A power law used to model the effective a-spot radius behavior as a function of temperature is [37]

$$a = CT^m \tag{3.12}$$

Equation (3.12) can alternately be expressed as the linear equation

$$y = mx + b \tag{3.13}$$

where y is ln(a), m is the slope, x is ln(T), and b is intercept, equal to ln(C). For each test sample, the corresponding values of ln(a) and ln(T) were plotted, estimating the coefficients with a linear regression analysis, as shown in Table 3. The model for the effective a-spot radius of a contact at a given temperature was defined as

$$a = T^m e^b \tag{3.14}$$

Table 3. PoF parameters for test samples

Sample	m	b
1	-1.65	16.93
2	-1.73	17.33
3	-1.91	18.38
4	-1.78	17.67
5	-1.97	18.72
6	-2.09	19.43
7	-1.67	16.89
8	-1.81	17.74
9	-1.89	18.11
10	-1.99	18.71

3.3.4 Model Validation

The reliability evaluation used to demonstrate the methodology consisted of a 0/110 ºC temperature cycle test, having 20 minute dwell times at each extreme, and 8 minutes of ramp time. The daisy chain resistances, as illustrated in Figure 13, were continuously monitored every 20 seconds.

From a pragmatic point of view, it was not possible to directly monitor the temperature of each IC socket contact during the experiment. Therefore, a single thermocouple was installed on the test board, one inch away from the contacts. An important consideration for temperature cycle evaluations is that the temperature of an IC socket contact lags behind that of the test board and the test chamber, a result of thermal gradients, and thermal mass effects. To accurately estimate the maximum resistance, it is necessary to quantify the difference between the contact and sensor at the peak of the temperature cycle. The temperature gradient (ΔT), between the elastomer contacts and the thermocouple, was estimated using the PoF model (3.14),

and the maximum contact resistance during a temperature cycle. For each maximum contact resistance (R_m), an expected temperature value was obtained, resulting in the temperature gradients shown in Table 4.

Table 4. Average temperature gradients for contacts at the maximum cyclic temperature

Sample	ΔT
1	9.2
2	8.7
3	8.8
4	9.2
5	7.5
6	8.6
7	7.8
8	8.4
9	8.3
10	9.1

On average, the maximum contact temperature was found to be 9 °C below that of the thermocouple. An updated PoF model, which incorporates the thermal gradient between the thermocouple location (at temperature T_m) and the contact (at temperature T'), is given by

$$R_{e'} = \frac{\rho_{T'}}{2a'} \tag{3.15}$$

where $\rho_{T'}$ is resistivity (estimated with maximum contact temperature T'), and a' is the effective a-spot radius at temperature T'.

Following the quantification of the thermal gradients, the temperature cycle test was started, and contact resistance values were continuously monitored. The cyclic resistance of all samples was found to decrease during the first 70 test cycles, stabilizing after 100 cycles. Previous experiments on this contact technology have

also shown similar contact resistance decreases as a function of time and temperature [38]. Therefore, the PoF model validation, and the definition and training of the SPRT were performed using test data from test cycles 100 to 124 (monitor cycles 0 to 24).

For each test cycle, the maximum temperature was measured; using the updated PoF model (3.15), a maximum resistance ($R_{e'}$) was estimated. For all 25 validation cycles, the resistance estimates were found to be within 0.05mΩ from the maximum contact resistance.

3.3.5 SPRT Definition and Training

The mean, and standard deviation of the resistance residuals (Δ_R) were estimated using data from the 25 validation cycles. The mean μ_0 was found to be 0.0mΩ (as expected), with a standard deviation σ = 0.01mΩ. These values represented the null hypothesis H_0, or the resistance residual distribution that was considered healthy. The mean for the alternative hypothesis was set to μ_1 = 0.1mΩ (0.1 mΩ above healthy residual mean), with standard deviation σ = 0.01mΩ (same as healthy residual σ). The false, and missed alarm probabilities were both set to 0.001. The SPRT index, assuming a normal distribution for n resistance residuals, is given by

$$-6.90 < 1000 \cdot \sum_{i=1}^{n} \left(\Delta_{Ri} - 0.05\right) < 6.90 \tag{3.16}$$

3.3.6 Resistance Monitor

The test board temperature and resistance of ten samples were continuously monitored for 500 temperature cycles, after the resistance values were stable (monitor cycles 0 to 500). For each cycle, the maximum contact temperature and resistance of each sample were identified, a maximum resistance was estimated with the model (3.15), and a resistance residual (Δ_{Ri}) was evaluated with the SPRT index (3.16).

Table 5 illustrates the monitoring results for one representative contact. After 114 monitor cycles, the resistance residual was considered "healthy," having values consistent with the null hypothesis [follows $G(\Delta_R)$ in Figure 10]. During monitor cycles 115-117, the residual status changed to "Unknown," having values between limits "A" and "B" of Figure 10. In monitor cycle 118, the resistance residual (Δ_{R118}) was found to be "Degraded" (follows $F(\Delta_R)$ in Figure 10). After 119 monitor cycles, the residual was considered "Healthy" again. The SPRT continued to produce intermittent alarms in this fashion until monitor cycle 156, when the alarms became continuous (a continuous alarm was defined as 5 or more continuous measurements that exceed the SPRT limit). As shown in Table 5, the M-SPRT methodology was capable of producing very accurate resistance estimates, and of detecting small changes in resistance behavior. Given that the PoF model considered the effects of temperature on the contact resistance, the accuracy of the estimates was not compromised either by thermal variability or by measuring error of the test setup.

Table 5. Resistance monitor results of sample 5

Monitor Cycle	T_m (°C)	R_m (mΩ)	R_e (mΩ)	CONTACT STATUS PER SPRT
26	96.1	7.79	7.77	**Healthy**
27	96.2	7.78	7.77	**Healthy**
28	96.1	7.78	7.77	**Healthy**
~	~	~	~	~
114	96.1	7.81	7.77	**Healthy**
115	96.0	7.81	7.77	*Unknown*
116	96.1	7.82	7.77	*Unknown*
117	96.0	7.81	7.76	*Unknown*
118	96.0	7.82	7.77	**Degraded**
119	96.1	7.81	7.77	**Healthy**
120	96.1	7.82	7.77	*Unknown*

* The digits for contact resistance are displayed for technique illustration purposes, showing the subtle and consistent shift in resistance that was observed in the experiment

Table 6 summarizes the results of the SPRT for all test samples. Six contacts were found to decrease their resistance during the experiment, requiring new model validation, and retraining of the SPRT. A new set of training measurements were acquired, model parameters were estimated, and new SPRT index equations were defined, just as illustrated by the loop to step 3 in Figure 11. The remaining four samples were found to have *s*-significant increases in resistance, which were consistent with the alternative hypothesis. In all cases, the increases in resistance were detected in less than 120 cycles.

Table 6. Contact resistance monitor results for temperature cycle test

Sample	Resistance Status	Cycle to 1st Alarm	Cycle to Continuous Alarm*
1	Decreased	--	--
2	Decreased	--	--
3	Decreased	--	--
4	Decreased	--	--
5	Increased	118	156
6	Increased	58	82
7	Increased	46	52
8	Increased	63	74
9	Decreased	--	--
10	Decreased	--	--

* A continuous alarm is declared when 5 or more continuous measurements exceed SPRT limit

3.4 Conclusions

A PoF-SPRT methodology was presented for the modeling and monitoring of resistance in electrical interconnects. The methodology, applicable for reliability and health monitoring applications, was demonstrated for an accelerated test using an IC socket assembly.

The resistance behavior of an IC socket contact was characterized at multiple temperatures. The contact resistance was found to increase as a function of temperature, from 4.8 mΩ at 25°C to 7.5 mΩ at 75°C. Contact characterization data is important for reliability, health monitoring, and electronic prognostic applications because it describes the “healthy” behavior of the electrical interconnect, and enables the selection and definition of physics of failure models.

A physics of failure model, based on the effective a-spot radius, and the resistivity of Ag, was developed for the elastomer socket. In addition, a power law model was developed to represent the behavior of the a-spot radius. The PoF model was used to provide resistance estimates as a function of temperature, and was shown to be highly accurate. This modeling approach is very useful for reliability and health monitoring applications because it produces low estimate errors, and because it takes into consideration the changes in contact resistance that result from thermal variability.

A SPRT was used to analyze the residuals (Δ_{Ri}) between the maximum resistance measurements (R_m), and the PoF model estimates (R_e). The M-SPRT approach provides high sensitivity for the detection of resistance degradation events, while allowing the selection of false and missed alarm probabilities. These advantages are not provided by traditional threshold-based methods. This methodology can be used to reduce test time requirements in reliability evaluations, and to provide early detection of precursors of failure in health monitoring, and electronic prognostic applications.

Chapter 4: Assessing the Reliability of Elastomer Sockets in Temperature Environments

4.0 Introduction

Land Grid Array (LGA) sockets are used in enterprise servers to interconnect integrated circuits (ICs) with printed circuit board (PCB) assemblies. These components offer an upgradeable, repairable, high density, and low cost alternative to solder joints [4], [6].

The current common LGA sockets consist of an array of contacts in a polymer housing that is compressed between the IC and the PCB. Three typical socket-contact technologies are stamped metal, fuzz button, and elastomer. Elastomer contacts in particular are composite structures where a carrier (elastomer) is filled with metal particles (Ag). The shape and density of these filler particles are designed to optimize mechanical and electrical properties. Elastomer contact technology is similar to conductive adhesive joints, with the difference that it provides a separable interconnection [30]-[34], [39].

In operation, mechanical loads are applied to IC sockets to compress the contacts between metal pads and to create microscopic contact areas called a-spots. When elastomer sockets are compressed, the contact expands perpendicular to the applied force, creating multiple Ag-Ag particle contacts. As the mechanical load increases, so does the effective a-spot area (the true contact area), with a resulting decrease in interconnect resistance [15], [40].

The mechanical and electrical characteristics of elastomer sockets have been discussed extensively in literature. Liu *et al.* [41] studied the effects of thermal and mechanical stresses on the contacts (10-100 g, -55 to 150 °C), finding that resistance behavior is strongly dependent on temperature and load.

Yang *et al.* [42] analyzed creep and stress relaxation failure mechanisms (with force and deformation-controlled assemblies), using socket coupons and an automatic contact-resistance probe. Creep, or time-dependent deformation, was found to reach 20-37% for temperatures between 40 °C and 150 °C (60-min exposure). Stress relaxation, or load loss over time, reached 30%-40% for temperatures between 40 °C and 125 ºC (100-min exposure). Contact resistance was estimated using a time-dependent stress relaxation model, material hardness, and resistivity.

Yang *et al.* [7] performed electrical bias experiments to assess electro-chemical migration (ECM). Highly accelerated stress test and 85°C/85% relative humidity (RH) experiments were performed. Silver ECM was produced with 5 V bias, causing a decrease in surface insulation resistance, from 10^9 to less than $10^5\Omega$ after 60 min of exposure.

Xie *et al.* [43] researched stiffness and stress relaxation behavior of contact coupons under mechanical load and over temperature (10-100 g, 26 °C-183 ºC). Temperature increases were found to decrease stiffness by 50% and to increase the contact force relaxation by 50% after 1 h at 133 ºC.

Xie *et al.* [20] assessed the operating reliability of a 787 contact socket, performing resistance measurements at multiple mechanical load settings. Test results

were fitted to an inverse Gaussian distribution, with the socket reliability for a 20 mΩ resistance requirement estimated at 99.3%.

Lie *et al.* [21] researched reliability issues such as high temperature dependence of resistance, high coefficient of thermal expansion, force deflection, stress relaxation, deformation, and adhesion. They suggested that under some conditions, elastomer contacts can exhibit electrical opens and shorts and intermittent behavior during operation.

Liu [44] investigated the effects of moisture and corrosive gas exposure on contact resistance. Elastomer sockets were found to be very resistant to moisture attack (140 ºC/85%RH), having no swelling and no significant increase in resistance after 150 h test. A mixed flowing gas environment (MFG class II) did not result in detectable increases of resistance.

Previously, the operating temperature and RH environment for IC sockets in an enterprise server application was quantified [19], and a temperature-dependent physics-of-failure (PoF) model for the contact resistance was developed [12].

The reliability of elastomer sockets during the first year of life after assembly has not been discussed in the literature, with most studies concentrating on contact behavior over short periods of time. This paper investigates the reliability of elastomer sockets in temperature conditions that are representative of postassembly storage, enterprise server operation, and mild accelerated testing. The paper also discusses the resistance behavior as a function of time and temperature, and the assessment of contact reliability with a PoF model and a log-normal distribution.

4.1 Contact Resistance Distribution

The resistance of electrical contacts is fitted to statistical distributions to estimate the probability that a given resistance value will be exceeded. Distribution functions typically used to model contact resistance behavior are the normal, log-normal, and inverse Gaussian, with normal distribution being applicable when symmetric behavior exists [20]. The cumulative density function, in terms of electrical contacts, provides the probability that a given resistance value will be observed in a series of measurements. To assess the goodness-of-fit of these distributions to experimental contact resistance data, a Kolmogorov-Smirnov test was used.

4.2 Experimental Setup

4.2.1 Hardware

IC sockets require load assemblies in order to provide low and uniform resistance connections between the LGA package and PCB pads. The experimental assembly consisted of a heat sink, screws, springs, thermal interface material, ceramic LGA package, IC socket, PCB, insulating Mylar film, and bolster plate [9], as shown in Figure 14. A study of the assembly component dimensions and spring constants estimated the applied load to be at 78 g per contact (see Appendix II). Shadow Moiré analysis of the LGA packages and bolster plates confirmed that the load-bearing surfaces met assembly flatness specification, a requirement needed to ensure load uniformity across all socket contacts (see Appendix III).

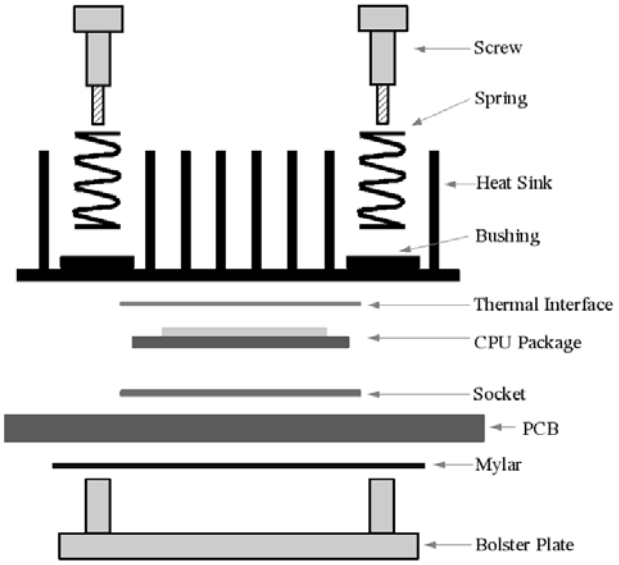

Figure 14. Illustration of the load assembly components used for the experiment. The socket is compressed between the LGA package and PCB pads

Tyco 1.0 elastomer sockets were used to interconnect ceramic daisy chain packages with PCBs. The socket is a 37 x 37 array of Ag-filled elastomer contacts, molded into a Kapton polyimide film and a thermoplastic housing, as shown in Figure 15. The daisy chain package and test-board assembly enable four-wire resistance measurements for 22 short chains, each one with two contacts in series, as shown in Figure 16.

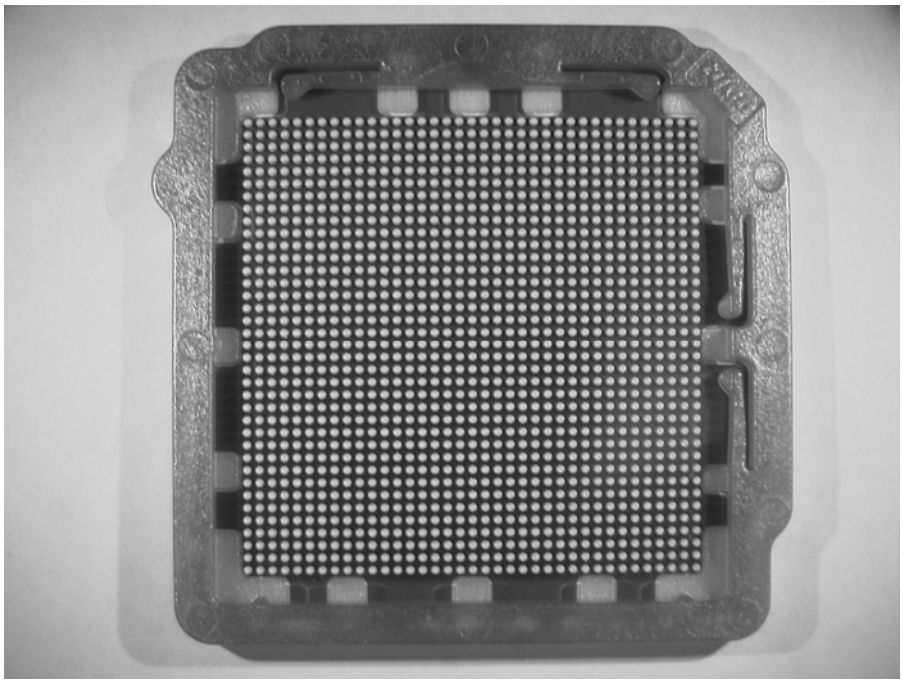

Figure 15. Illustration of an elastomer socket showing the 37 x 37 array of contacts, Kapton film (dark regions between contacts), and thermoplastic housing (perimeter)

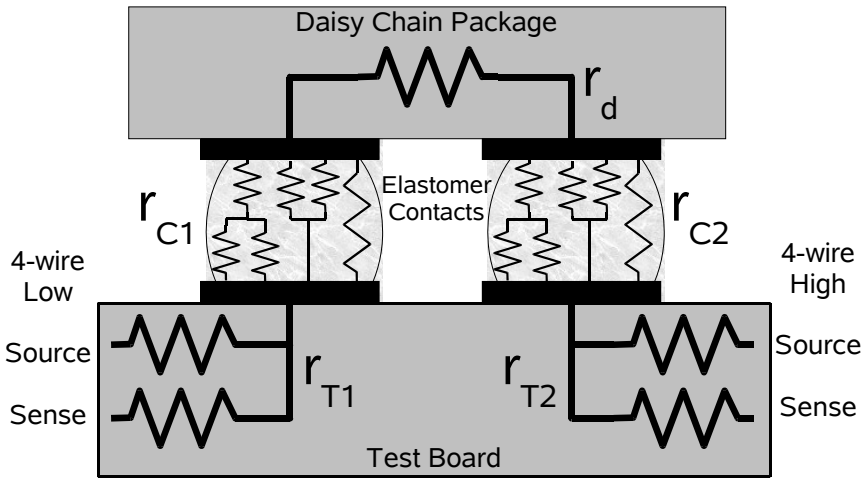

Figure 16. Illustration of a two-contact chain formed by the test assembly and the IC socket. Four-wire method is used for resistance measurements. r_{c1} and r_{c2} are the contact bulk resistance. r_{T1} and r_{T2} are the test board circuit resistance. r_d is the package resistance. The resistance network inside contacts represents that of Ag-Ag particle contacts

Resistance values across the short chains (r_m), measured with a Keithley 580 micro Ohm meter, consist of contact-pad, contact bulk (r_{c1}, r_{c2}), package (r_d), and test board (r_{T1}, r_{T2}) resistances. Contact to pad resistance (Au-Ag) is very small in relation to bulk resistance. Therefore, the test circuit resistance ($r_d+r_{T1}+r_{T2}$), was found to be 16.7 mΩ. The resistance of an individual contact r_c, as a function of the measured four-wire resistance r_m, is estimated by

$$r_C = \frac{r_m - 16.7}{2}. \tag{4.1}$$

A repeatability study was carried out to assess the measuring system error. The study performed 30 measurements, with and without repositioning of test probes, finding the maximum variability of the measurements to be less than 0.05 mΩ from the mean.

4.2.2 Experimental Groups

The resistance behavior of elastomer contacts was evaluated with three temperature conditions: 25 °C, 55 °C, and 75 °C. All test groups were assembled with the hardware described in section 4.2.1. The sample sizes for the experiment are provided in Table 7. Test group 1 (25 °C) evaluated the contact behavior of sockets that are assembled (mechanically loaded) and kept in storage for weeks or months before first use. This condition simulates the aging of sockets in systems or modules that are stored by the manufacturer (presale), customer (postsale), or field service engineer [Field Replaceable Units (FRUs)]. Some customers can also store systems as replacement units for safety-critical applications. Test group 2 (55 °C) evaluated the behavior of mechanically loaded sockets at common operating temperature, based on

previous studies of enterprise server applications [19]. This condition allows the study of thermal effects on contacts during operation, without the influence of electrical bias. Test group 3 (75 °C) evaluated sockets at an accelerated load condition. The temperature was chosen to reduce overacceleration effects which can introduce mechanisms or behavior not relevant for nominal operating conditions. This consideration was important due to the documented complex behavior of the elastomer socket [7], [20], [21], [41]-[43].

Table 7. Sample sizes for experimental test groups

Group	Temperature	Test Boards	Daisy Chains
1	25 ºC	7	154
2	55 ºC	7	154
3	75 ºC	4	88

4.2.3 Test Procedure

Samples from group 1 were assembled, the resistance measured, and stored in an office environment (~25 °C). Samples from groups 2 and 3 were assembled, measured, and placed inside temperature chambers at 55 ºC and 75 °C, respectively. At predetermined time intervals the samples, from all test groups were taken out of their test conditions, allowed to dwell at room temperature for 1 h, measured, and returned to their respective test environment.

All groups were tested for 2000 h. Selected samples from groups 1 and 3 were further tested to provide insight into the contact behavior during the first year of life. Group 1 samples (88 contacts) were tested up to 16 500 h. Group 3 samples (88

contacts) were tested up to 4500 h. Group 2 samples were not tested beyond 2000 hours.

4.3 Results and Discussion

4.3.1 Resistance Behavior

The contact resistance measurements from the three test groups were fitted to normal, log-normal, and inverse Gaussian distributions. None of the assumed statistical distributions provided an acceptable fit for the 25 °C data, which exhibited nonlinear behavior on probability plots. Fitting to other statistical distributions, such as Weibull, was also unsuccessful. A closer examination of the data showed that the observations were the result of a mixed population and having two modes and a mixed/transition period. An excellent fit was obtained using a three-population mixed-Weibull distribution model, as shown in Figure 17.

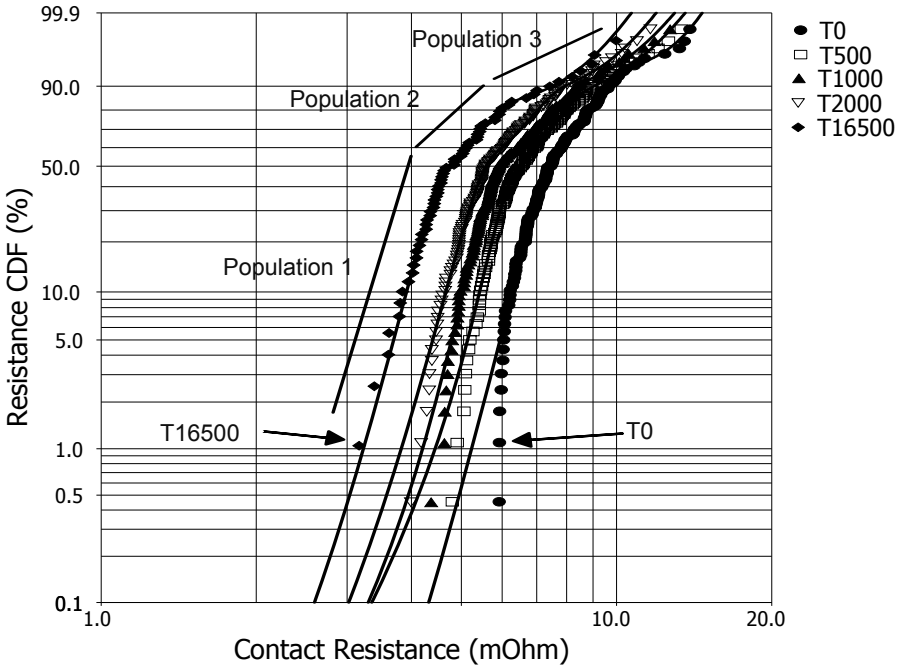

Figure 17. Three-population mixed-Weibull probability plot for resistance of elastomer contacts evaluated with 25 ºC condition. Measurements and fit lines for 0, 500, 1000, 2000, and 16500 h are shown

Population 1 consists of the samples in the high slope portion of the curves. Population 3 consists of the samples in the low slope portion of the curves. Population 2 is the knee/transition region. Measurements at T0, T500, T1000, T2000, and T16500 hours are shown. The average contact resistance for the samples in the 25 °C condition decreased 25% after 2000 h. Using the mixed-Weibull model, it was estimated that, after 16500 h, approximately 40% of the samples (population 1) had a Weibull slope $\beta=14$, and 20% (population 3) had a Weibull slope $\beta=6$.

In elastomer sockets under applied loads, there is significant amount of viscoelastic deformation, which can result in stress relaxation if the structural configuration constrains the deformations in any way. When an elastomer contact is mechanically loaded, the elastomer portion of the matrix starts to creep, resulting in

contact radial expansion and height reduction. After the socket stops are reached (which are provided to prevent overloading), the assembly is constrained from further deformation and the stresses progressively relax in the elastomer. Furthermore, the applied mechanical loads are transmitted by the elastomer matrix to the silver particles distributed throughout the matrix. These Ag particles can then experience physical contact with neighboring particles, creating microscopic contact regions called a-spots. As the elastomer undergoes stress relaxation at an average macroscale, the applied mechanical stresses can internally redistribute, resulting in increased contact stresses at the microscale, between the Ag particles. This increasing contact stress can lead to an increase of the effective contact area between the Ag particles, particularly if the Ag undergoes any creep deformation at this temperature. The net effect is a reduction in contact resistance over time, although the average stress in the elastomer interconnect appears to decrease at the macroscale.

In the test assembly utilized for this experiment and with the 78 g load applied, the elastomer creeps rapidly (within minutes) until the socket stops are reached. Test results show that contact resistance decreases over time. Elastomer stress relaxation, which causes an increase in contact resistance, is not a predominant mechanism within this timeframe of the loading conditions. Cross-sectional analysis of a socket assembly at the beginning of the experiment confirmed that the socket stops had been reached. The observed reduction in resistance results from an increase in the effective contact area between the Ag particles, either from an increase in area of the existing Ag-Ag a-spots or from the creation of additional a-spots. Population 1 in Figure 17, exhibiting the greatest decrease in resistance over time, represents the

fraction of the elastomer contacts where an increase of the effective a-spot area is the dominant mechanism. Population 3 in Figure 17, exhibiting higher resistance values over time, represents the fraction of the contacts where elastomer relaxation is becoming a more dominant mechanism. More studies are necessary to further investigate this behavior.

The changes in statistical distribution exhibited by samples in the 25°C condition (Figure 17) are of concern for the long-term reliability of the socket. As the contact ages, this behavior could result in a rapid decrease of reliability over time, particularly for units that have been assembled and stored for over a year.

The 55 °C data (up to 2000 h) exhibited linear behavior in the probability plots and was fitted with a log-normal distribution, as illustrated in Figure 18. The average contact resistance decreased 20% during the first 500 h and 35% after 2000 h. The shape parameter increased 30% in the same period, changing the distribution shape from normal to log-normal. The 75 °C data displayed nonlinear resistance behavior in a log-log plot, particularly after 500 test hours. A three-parameter Weibull distribution was found to provide an acceptable fit to the data up to 2900 h, as illustrated in Figure 19. For the 4500 h data, a mixed-Weibull model provided a better fit. Notice in Figure 19 the changing distribution slope over time, which suggests a degrading reliability. Overall, the mean contact resistance decreased 45% in the first 500 h and 50% after 2000 h. The added reduction in resistance in this test group, when compared to that observed in the 25 ºC and 55 ºC groups can be explained by the higher stress temperature, which induces lower stiffness (elastomer), higher thermal expansion (elastomer, Ag, and assembly), and higher stresses (between Ag

particles). The change of distribution to a mixed-Weibull model at 4500 test hours indicates a change in the dominant mechanism, from a Ag particle-related mechanism, to elastomer stress relaxation.

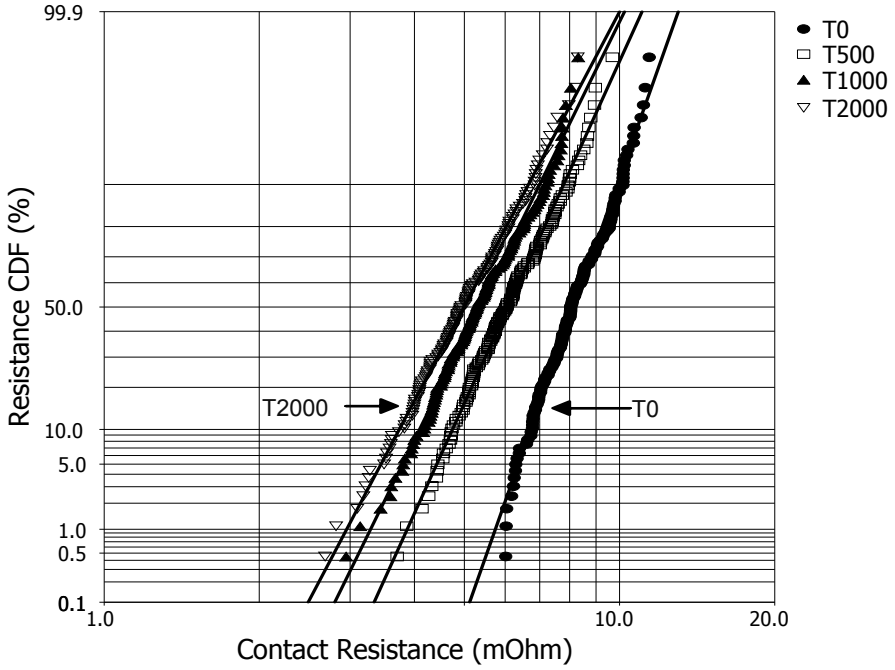

Figure 18. Log-normal probability plot for elastomer contact resistance evaluated with 55 ºC condition. Measurements and fit lines for 0, 500, 1000, 1500, and 2000 h are shown. The resistance behavior is linear in the logarithmic scale. Each data set consists of 154 measurements

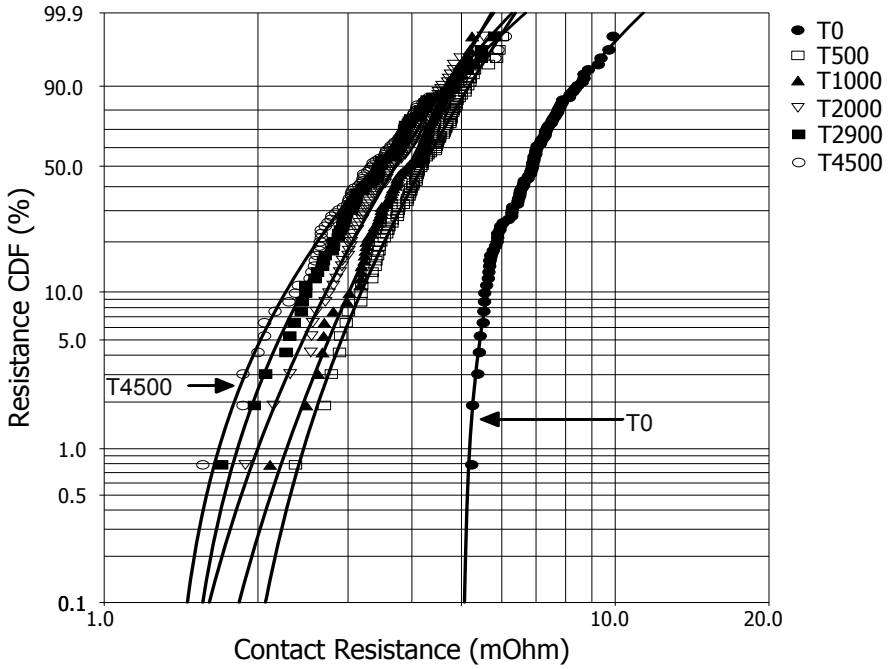

Figure 19. Three-Parameter Weibull probability plot (uncorrected for gamma) for elastomer contact resistance evaluated with 75 ºC condition. Measurements and fit lines for 0, 500, 1000, 2000, 2900, and 4500 h are shown

Test results show that while the temperature used for test group 2 (55 °C) was able to drive a consistent and stable contact aging, this is not the case for higher or lower temperatures. Accelerated tests on this contact technology can produce behavior and failures that are not present under nominal operating conditions. If the temperature is too low or too high, the effect of Ag particles in the matrix can be underestimated or overestimated. Therefore, over acceleration of elastomer contacts can mask the true long term effects of elastomer stress relaxation.

While the resistance behavior is represented by multiple statistical distributions, it is possible to model the mean contact resistance over time and temperature. Mean resistance values for all test groups and times were calculated,

with results provided in Table 8. Values for extended test times (2900, 4500, 16 500 h) are also included.

Table 8. Mean contact resistance for test group data

Time	μ (mΩ) 25 ºC	μ (mΩ) 55 ºC	μ (mΩ) 75 ºC
0	7.8	8.2	7.0
500	6.9	6.2	4.2
1000	6.5	5.5	3.9
1500	6.2	5.2	3.7
2000	6.0	5.1	3.7
2900			3.5
4500			3.5
16 500	5.2		

4.3.2 Time-Dependent Model for Mean Contact Resistance

The resistance of an elastomer contact is a function of the true contact area (effective a-spot), the resistivity of silver, and the stress relaxation of the elastomer. Since the elastomer relaxation is not a predominant mechanism for the temperature conditions utilized in this experiment, the model will be defined only as a function of the contact area and resistivity of Ag. A model to describe the mean contact resistance is [42]

$$\mu = \frac{\rho_T}{2a} \tag{4.2}$$

$$\rho_T = \rho_{20} + \rho_{20} * (T - 293.15) * \gamma \tag{4.3}$$

where μ is contact resistance (Ω), ρ_T is resistivity of Ag as a function of temperature, a is effective a-spot radius (true contact area radius), ρ_{20} is resistivity of Ag at 20 °C,

T is temperature of the contact in Kelvin, and γ is thermal coefficient of resistivity for Ag (0.0038).

Lopez *et al.* [12] showed that the true contact area of an elastomer contact decreases as a function of temperature (higher temperature equals higher resistance), and that the behavior was consistent with a power law model. The results of this research show that the true contact area increases as a function of time (resistance decreases), resulting from increased contact stresses between Ag particles in the matrix. An analysis of the data from Table 8 showed that the effective a-spot radius, derived from the mean contact resistance over time, was also consistent with a power-law model

$$a = Ct^m \tag{4.4}$$

where C and m are constants and t is test time in hours. Taking the natural log of (4.4)

$$y = mx + b \tag{4.5}$$

where y is ln(a), m is the slope, x is ln(t), and b is intercept, equal to ln(C). A linear regression analysis of the x versus y plot, using the experimental data for each test condition up to 2000 h, provided the coefficients m and b. For convenience, the a-spot radius as a function of time is represented by (4.6), with values for the model parameters m and b provided in Table 9

$$a = t^m e^b. \tag{4.6}$$

Table 9. Parameters for PoF model – three groups

Test Group	m	b
1	0.085	-14.16
2	0.111	-14.18
3	0.097	-13.74

The model given by (4.2), (4.3), and (4.6) was used to estimate the mean contact resistance of the elastomer socket and is plotted against experimental results shown in Figure 20. For all test groups and test times, the model estimates were within 3% of actual observations. Extended test results for groups 1 and 3, which were not used to create the model, were also found to be within 3% of the estimates. See Appendix VI for a generalized form of the model.

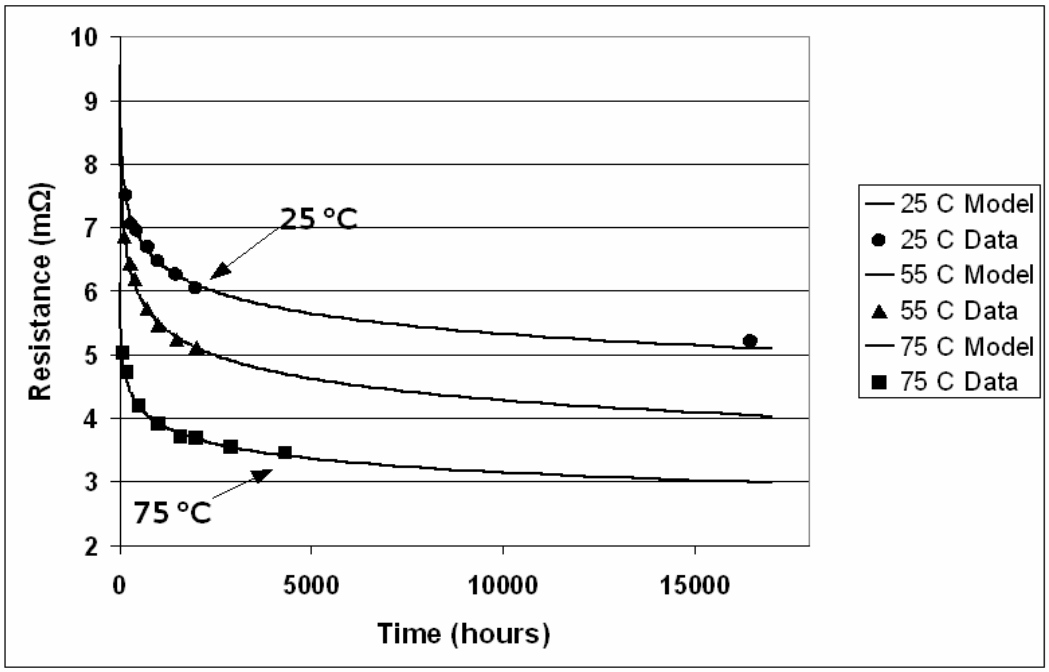

Figure 20. Plot for the mean contact-resistance model as a function of time for 25 ºC, 55 ºC, and 75 ºC conditions. The model estimates (fit lines) and experimental measurements (markers) are shown. Notice the model fit for extended test results at 75 ºC (2900 and 4500 h, lower curve) and 25 ºC (16 500 h, upper curve)

4.3.3 Contact Reliability

The contact resistance behavior at normal operating temperature can be estimated with a log-normal – power-law relationship

$$f(r) = \frac{1}{\sqrt{2\pi}\sigma' r} e^{-\frac{[\ln(r)-\mu']^2}{2\sigma'^2}} \tag{4.7}$$

where r is contact resistance, σ' shape parameter, and μ' the mean of the natural log of resistance [estimated with (4.2), (4.3), and (4.6)]. The reliability of the elastomer contact and socket were estimated assuming a resistance requirement of r ≤ 20 mΩ, nonbias operation at 55 ºC, and a series reliability model [27]. For the first year of operation, the reliability was determined to exceed 99.99% for both contact and socket, as shown in Table 10.

Table 10. Estimated reliability for first year under nonbias conditions

Elapsed Time	Log-normal Shape* Parameter	Estimated Mean** Resistance (mΩ)	Contact Reliability	Socket Reliability (1369 contacts)
1 Month	0.202	5.59	>99.99%	>99.99%
3 Months	0.226	4.93	>99.99%	>99.99%
6 Months	0.235	4.56	>99.99%	>99.99%
12 Months	0.240	4.22	>99.99%	>99.99%

* Shape parameter values from test data. Six and twelve month parameters estimated from extended test results (16500 hours at 25 ºC and 4500 hours at 75 ºC).

** Mean resistance estimated with PoF model described in section 4.3.2

While the first year reliability is high, it was shown that the contact has changes in the resistance distribution over time and temperature that are not desirable for the long term reliability of the socket. As the contact ages and elastomer stress

relaxation becomes a dominant mechanism, the observed distribution changes will reduce product reliability by increasing the probability of higher resistance values. For the case of elastomer sockets that are assembled and stored at room temperature before first use (as in backup systems, replacements in safety critical applications, FRUs, and spare assemblies), the contacts will experience a significant increase in the probability of failure after 2000 h.

Socket assemblies tested at 55 ºC condition display an increase in the probability of failure as a result of steady increases in the log-normal shape parameter, from 0.15 at the beginning of the test and up to 0.23 after 2000 h (seen as decrease in slope over time in Figure 18). At 75 °C, there is also a decrease in slope over time. The decrease in slope results in an increased probability of contact failure over time, which is an important factor for high-density IC sockets (1500+ contacts) and multisocket systems.

4.4 Conclusions and Recommendations

This paper investigated the resistance behavior of metal-filled elastomer sockets that were mechanically loaded and subjected to non-bias temperature conditions representative of postassembly storage, normal temperature operation, and accelerated testing conditions. Contact resistance was shown to decrease as a function of time and temperature after 2000 test h (25% at 25 ºC, 50% at 75 ºC). This decrease in resistance should be considered in quality, reliability, and health-monitoring applications to define baseline resistance characteristics and to improve failure detection sensitivity.

The resistance of sockets evaluated at 25 ºC (postassembly) was found to follow a mixed-population Weibull distribution. This condition was shown to be undesirable for long-term socket reliability because it increased resistance variability over time, which can result in unacceptable increases in the occurrence of failure. It is recommended that elastomer socket assemblies, as the ones described in this study, should not be stored for long periods of time (months) before first use.

The resistance of sockets evaluated at 55 ºC (common operating temperature) showed linear behavior in the log-log scale, with a log-normal distribution providing the best fit. The log-normal scale parameter was found to increase over time, changing the distribution shape and gradually increasing probability of higher resistance values. The resistance behavior of sockets evaluated at 75 ºC (accelerated temperature) was best fitted by a three-parameter Weibull distribution. The distribution parameters for this condition were also found to vary over time. Changing parameters in the statistical distribution of resistance are important reliability indicators. These parameters should be closely monitored in IC socket evaluations to allow an understanding of trends and potential failures of the contact technology.

The test results show that the contact resistance behavior of elastomer sockets is defined by multiple statistical distributions over temperature and time. This statistical variation is an indicator of multiple active mechanisms on the elastomer contact. As a result, tests performed at conditions above or below the common operating temperature (55 ºC) could mask the effect of failure mechanisms and lead to erroneous conclusions. It is recommended that conditions used to evaluate

elastomer sockets are carefully reviewed to ensure that stress and stress levels are accelerating the desired behavior.

A PoF model of the mean contact resistance was developed and combined with a log-normal distribution to estimate the socket reliability. This is significant because the model can be used to estimate the probability of failure of an elastomer contact, socket, or sockets in a system, as a function of temperature and of contact age, in which probability is a key parameter to estimate system reliability. The model is suggested for first-level socket reliability estimates in enterprise servers.

Further experiments are required to study the effects of elastomer stress relaxation in the contact behavior during the second and third year of operation at common operating temperature. Other studies are also needed to assess the combined effect of temperature and electrical bias on the long-term reliability of this contact technology.

Chapter 5: Effects of Electrical Bias on Contact Resistance

5.0 Introduction

Electrical bias is a key element in the operating environment of IC sockets. In typical applications roughly 45% of contacts perform power and ground functions, while 55% perform signal and signal control functions. Understanding the effects of electrical bias is therefore important for any contact reliability analysis.

The research presented in Chapter 4 studied the contact resistance behavior of mechanically loaded contacts as a function of time and temperature. In this chapter elastomer contacts, also under mechanical load, were stress tested with 200, 250, 300, and 350 mA bias current, representative of nominal and accelerated operating conditions. The experiment monitored changes in resistance as a function of electrical bias and time.

5.1 Experimental Setup

As shown in Figures 17, 18, and 19 (Chapter 4), elastomer contacts under mechanical load display greater resistance variability when they are maintained at ambient temperature. Therefore, to maximize resistance degradation, and to minimize the effect of temperature on the contact, a test condition of 25 ºC was selected. Seven test boards with daisy chain packages (illustrated in Figure 13, Chapter 3) were wired and connected to a ballast resistor and power supply, as shown in Figure 21.

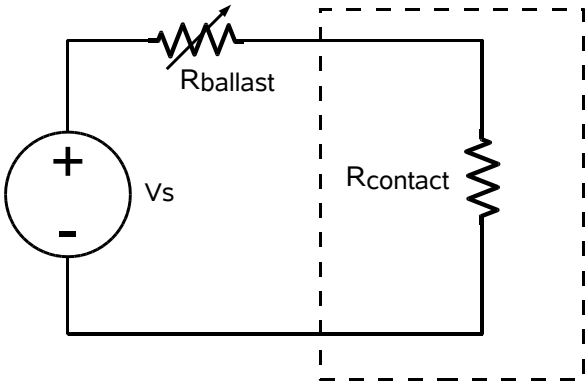

Figure 21. Test circuit for bias experiment. The power supply and ballast resistor are set to provide the required current flow for each test cell. The dashed line represents the thermal chamber (set to 25 °C)

From the daisy chain packages 16 samples were selected for electrical bias testing and 43 for control purposes. The location of all control samples was selected to be within 10mm from the bias samples, this to reduce the resistance variability that results from package surface effects. The contact resistance was measured for all samples at the beginning of the experiment and at predetermined intervals, up to 2000 hours. The test groups, sample sizes, and bias conditions are shown in Table 11.

Table 11. Test cells and sample sizes for electrical bias experiment

Cell	Bias Current (mA)	Sample Size	Comments
1	200	6	Nominal current
2	250	4	+25% current
3	300	4	+50% current
4	350	2	+75% current
Control	---	43	----------

5.2 Results and Discussion

The contact resistance measurements of the control samples were analyzed and fitted to Log-normal and Weibull distributions. A three-Parameter Weibull model was found to provide the best fit to the data, as illustrated in Figure 22. Notice that the resistance behavior is not identical to the one shown in Figure 17 (Chapter 4), for the 25º C condition. This behavior difference is attributed to the smaller sample size used in this experiment and to the selection of specific package locations for monitoring.

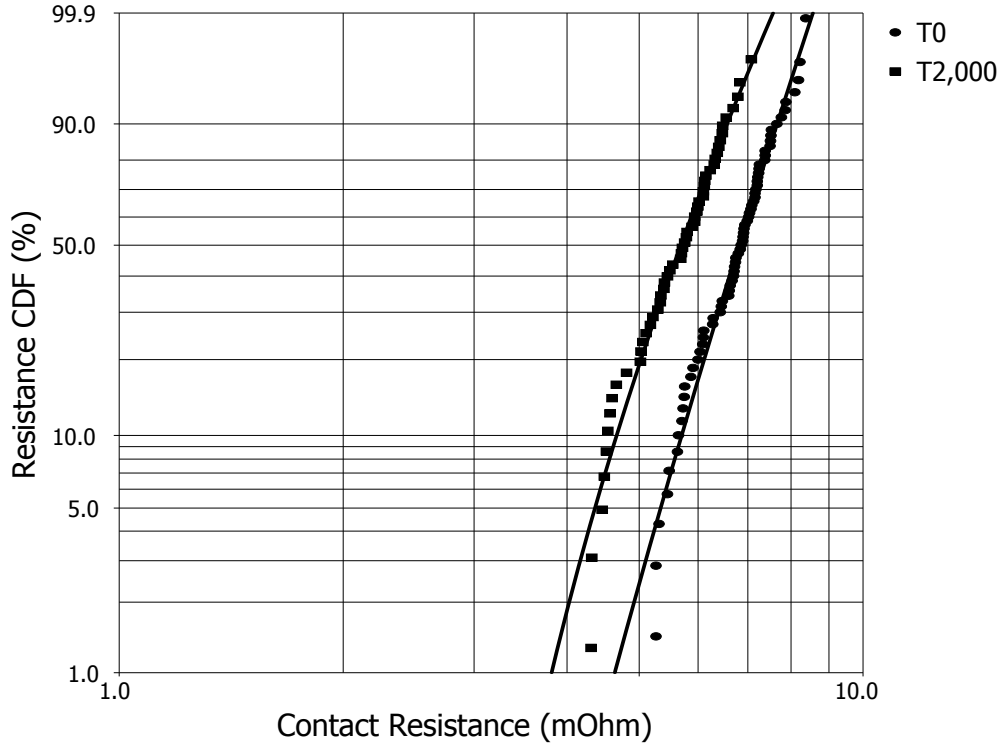

Figure 22. Three-Parameter Weibull probability plot of control samples at 25 ºC condition. Measurements and fit lines for 0 and 2000 hours are shown

The contact resistance of the control samples decreased an average of 18% (ranging from 9 to 29%) during the 2000-hour test, similar to the experimental results shown in Chapter 4, 25 °C condition. The resistance of the samples subjected to electrical bias also improved during the experiment, with decreases ranging from 11% to 35%. These values are similar to the ones observed in the control samples, not showing any indication of contact resistance increases resulting from the electrical bias. Test results are shown in Table 12.

Table 12. Electrical bias test results

Test Cell	Resistance Decrease (%) After 2000 h
200 mA	12,13,18,20,30,30
250 mA	21,23,33,35
300 mA	11,15,18,21
350 mA	14,14
Control	18% average

5.3 Conclusion

The elastomer contacts that were subjected to electrical bias, from 200 to 350 mA, did not display a detectable increase in contact resistance during the 2000-hour experiment. These results suggest that temperature and mechanical load are the key factors in elastomer contact resistance degradation (for this particular server application), as assumed by the models presented in Chapter 4.

Chapter 6: Sources of Failure in IC Socket Contacts

6.0 Introduction

To analyze the potential sources of failure for IC socket contacts it is imperative that a "life cycle" point of view be considered. By examining the different life phases it is possible to identify issues that result from the contact design, system design, system components, system assembly, transportation, operating environment, and socket-system interactions, among others. The sources of failure during the IC socket life cycle are illustrated in Figure 23 and will be discussed in the following sections.

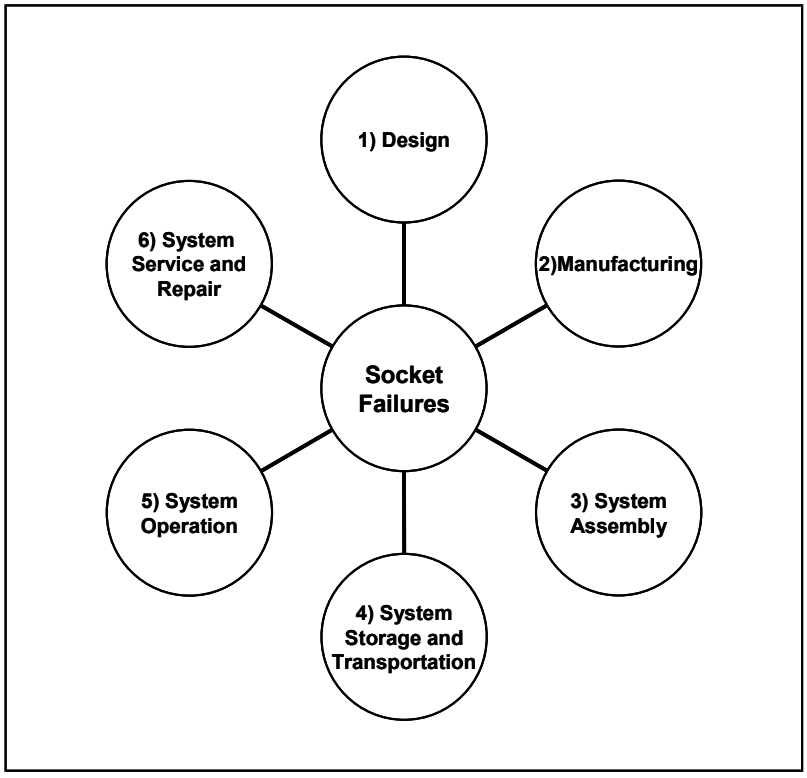

Figure 23. Sources of failure for IC socket contacts

6.1 Design

Design is the key contributor of failures for IC socket technologies [52]-[54]. Some IC sockets, such as the CIN::APSE® [55], are known in industry for their superior quality, reliability, and high cost. Other technologies, such as the metal-in-elastomer, are known in industry for their excellent quality, lower reliability, and low cost. For illustration purposes, the differences between these two socket technologies will be briefly discussed.

The Cinch CIN::APSE® socket consists of an array of buttons that are carried on a plastic housing. Each button is made of 7 bundled wires, that when compressed, provide physically independent, point-to-point, current paths. The contact absorbs 100% of the applied load, does not wipe the IC and PCB pad surfaces, and maintains its position during temperature excursions. An important feature of this design is that not all wires in a contact are required for successful operation. This contact design has embedded redundancy, which is used in high reliability systems. A SEM image of a CIN::APSE® contact is shown in Figure 24. A reliability block diagram that can be used to represent this contact technology is illustrated in Figure 25.

Figure 24. SEM SE (20KV, 300x) image of a Cinch CIN::APSE contact

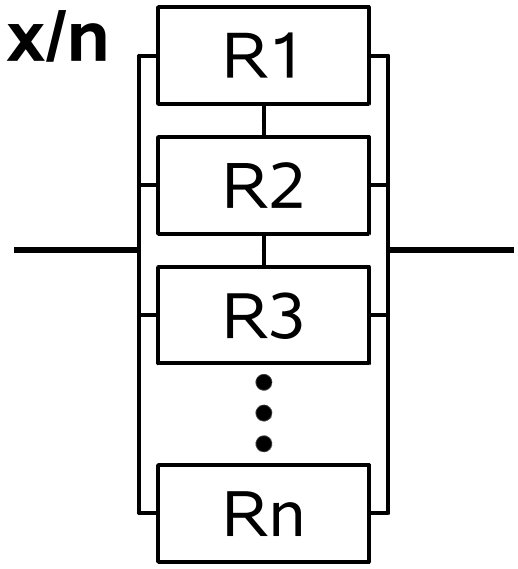

Figure 25. Reliability block diagram of an "x-out-of-n" system, representative of a CIN::APSE contact. ***x*** represents the minimum number of wires needed for successful operation and ***n*** represents the total number of wires

The elastomer socket consists of an array of buttons that are molded on top of a Kapton® film, and carried by a plastic housing. Each button is made of Ag-filled elastomer, that when compressed, provides hundreds of interconnected current paths.

Because it is a composite structure, any load applied to an elastomer contact is shared between the elastomer and the Ag particles. Just as CIN::APSE®, this contact technology does not wipe the IC and PCB pad surfaces. An important difference is that the elastomer contact does not maintain the position of the interconnected paths during temperature excursions. As the contact is heated up, the elastomer experiences radial expansion, and all Ag-Ag particle interfaces are gradually disrupted. This contact design has an embedded coupling factor (elastomer), which can result in lower socket reliability. A high magnification cross-sectional image of an elastomer contact, showing the elastomer and Ag particles, is shown in Figure 26. A reliability block diagram that can represent the elastomer contact is illustrated in Figure 27.

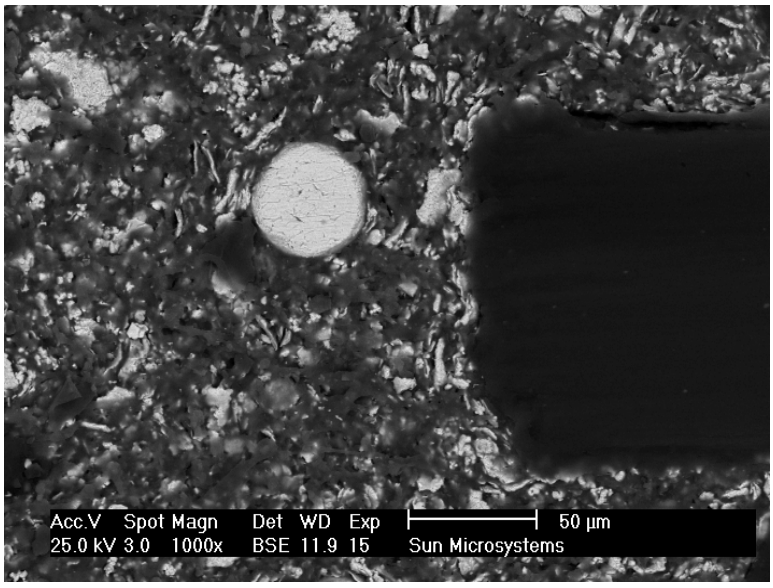

Figure 26. SEM BSE image (25KV, 1000x) of a Ag-filled elastomer contact cross section. The dark region on the middle-right is the Kapton carrier. The light colored areas are Ag. The dark colored areas are elastomer

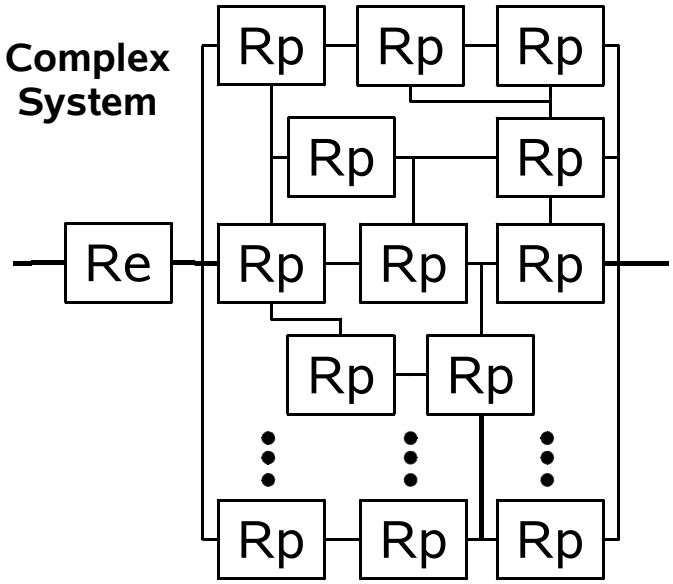

Figure 27. Reliability block diagram representing an elastomer contact. Re is the contact reliability due to the elastomer (coupling factor). Rp is the reliability of the contact due to the Ag-Ag particle interactions

From the brief technology descriptions above it is easy to see that a contact designed with embedded redundancy can be expected to have higher reliability than a contact designed with embedded coupling factors. The presence of a root cause and a coupling factor between components or systems is known in reliability literature as common cause failures (CCF) [56], which are found in low reliability systems.

Contrasting the characteristics that exist or do not exist in a contact technology can be an important tool for the identification of the sources of failure. With these considerations in mind, a list of design factors that can induce IC socket failures is shown in Table 13.

Table 13. Design factors that can induce socket failure

Socket	▪ Electrical function (DC power, ground, AC signal) ▪ Embedded redundancy (contact level) ▪ Resistance distribution behavior as a function of temperature and time ▪ Thermal stability of contact and housing ▪ Mechanical load vs. resistance response ▪ Socket size and contact count ▪ Distance of contact from package neutral point ▪ Socket stops and maximum allowed compression ▪ Sensitivity to mechanical load variation ▪ Contact wipe distance (stamp metal) ▪ Common cause factors designed into socket and contact ▪ Global alignment features ▪ Lateral loading/socket shift during assembly (contact orientation, load)
IC Package	▪ Designed redundancy at socket level ▪ Redundancy in power, ground, and signal lines ▪ Hardness and thickness of pad metal finish (stamp metal) ▪ Pad finish thickness vs. socket assembly cycles (exposure of base metal)
Mechanical Load Assembly	▪ Mechanical load variation as a function of operating environment (CTE, relaxation) ▪ Spring relaxation behavior over time
Printed Circuit Board	▪ Thickness and warpage of socket assembly under mechanical load ▪ Via design, location, and reliability under load ▪ Thermal gradients ▪ Surface finish under contact region

6.2 Manufacturing

Manufacturing defects or variability that can induce contact failures are typically detected by outgoing and incoming inspections. Nevertheless, it is not uncommon to have defects or out-of-specification material that escapes these inspections and produces a decrease of quality and/or reliability. Besides the obvious socket concerns it is important that LGA package, mechanical load assembly components, PCB, storage, and transportation factors are considered and monitored on a regular basis. These factors are provided in Table 14.

Table 14. Manufacturing factors that can induce socket failure

Socket	▪ Handling ▪ LCP flash ▪ Elastomer flash ▪ Knit lines, cracks, and crack propagation pattern ▪ "Improvement" of manufacturing process ▪ Changes of material or material supplier ▪ Changes of metal particle concentration and shape (elastomer) ▪ Contamination (fiber, dust, oil) ▪ Manufacturing variability (dimension)
IC Package	▪ Surface flatness, shape, and variation ▪ Pad finish defects
Mechanical Load Assembly	▪ Defective or out of specification components ▪ Component variability (excessive) ▪ Change of supplier ▪ Shape, flatness, and variation of bolster plate
Printed Circuit Board	▪ Contamination and/or factory residues
Socket Storage and Transportation	▪ Storage duration and environmental conditions ▪ Exposure to corrosive gases

6.3 System Assembly

IC sockets are not independent or isolated components of a system, but rather part of highly integrated assemblies. Failures can result from assembly specification issues, operator mistakes, material damage, contamination, and socket/assembly deformation after application of the mechanical load. These sources of failure are shown in Table 15.

Table 15. System assembly factors that can induce socket failure

Socket	▪ Handling damage ▪ Contact residue on pad ▪ Dust ▪ Improper socket seating ▪ Global or local misalignment ▪ Housing/carrier cracks ▪ Creep ▪ Rework damage ▪ Aligning post damage ▪ Contact tilt (due to via design and initial wipe)
IC Package	▪ Initial pad wear and under metal thickness/exposure (stamped metal)
Mechanical Load Assembly	▪ Mechanical load sequence (localized over/under loading) ▪ Load specification ▪ Load uniformity (contact to contact, board to board) ▪ Wrong, damaged, or missing assembly component
Printed Circuit Board	▪ Damaged pads ▪ Manufacturing process residue on surface

6.4 System Storage and Transportation

A socket assembly inside of a computer system can pass outgoing inspection at the manufacturing site, but fail to operate when it reaches the customer. Socket failures can be induced by inadequate storage conditions, long term storage (1+ years), or by extreme shock, vibration, and temperature exposure during transportation. These factors are shown in Table 16.

Table 16. System storage and transportation factors that can induce socket failure

Environment	▪ Exposure to elements (rain, uncontrolled temperature, and humidity) ▪ Rodents and insects
Socket	▪ Stress Relaxation ▪ Contact corrosion ▪ Housing cracking ▪ Shift of statistical distribution of resistance (under mechanical load)
IC Package	▪ Pad corrosion
Mechanical Load Assembly	▪ Relaxation of assembly component
Printed Circuit Board / Assembly	▪ Shock and vibration (transportation) ▪ Thermal shock (transportation)

6.5 System Operation

This section considers all factors that can have a negative impact on the reliability of the contact during normal system operation. The main areas of interest are environmental conditions, socket degradation, IC package, mechanical load assembly, and PCB, as shown in Table 17.

Table 17. Operating environment factors that can induce socket failure

Environment	▪ Temperature, humidity, and corrosive gas content of ambient air ▪ Air flow at socket interconnect and access of unheated ambient air (higher humidity, higher corrosive gas content) ▪ System fan effectiveness, degradation, and/or failure ▪ System vibration ▪ Operating life requirement (years)
Socket	▪ Temperature and humidity at socket contact interface ▪ Housing relaxation and outgasing ▪ Cyclic wipe over metal pads (stamped metal) ▪ Stress relaxation ▪ Statistical distribution of resistance over temperature ▪ Shift in statistical distribution of resistance over time ▪ Intermetallic formation and pad/contact fusion ▪ CTE mismatch between IC, package, and PCB
Electrical	▪ Electrochemical Migration (ECM) ▪ Joule heating and thermal runaway ▪ Bias and operating frequency (AC/DC)
IC Package	▪ Junction temperature ▪ Thermal gradients ▪ Power on/off cycle range and

	▪ Temperature cycle range and frequency/life ▪ Package pad damage and corrosion ▪ Cyclic pad wear
Mechanical Load Assembly	▪ Load relaxation (spring relaxation over time or temperature) ▪ Load relaxation (screw damage, screw loosening) ▪ Load shift (socket shift)
Printed Circuit Board	▪ Warpage over thermal profile and load

6.6 System Service and Repair

Systems are typically subjected to maintenance and repair activities. If the socket assembly is disrupted, to upgrade the IC component or to repair a socket issue, then it is possible to introduce potential IC socket failures. All assembly factors indicated in Table 15 should be considered, as well as those provided in Table 18.

Table 18. System service and repair factors that can induce socket failure

Socket Assembly	▪ Socket handling ▪ Socket removal process ▪ Assembly process
IC Package	▪ Socket residue on pad ▪ Pad wipe damage
Miscellaneous	▪ Unnecessary repair ▪ Wrong part (FRU)

6.7 Conclusions

The sources of failure for IC socket contacts are not restricted to those directly related to the socket design and manufacturing, but include system assembly and assembly components, system storage, operating environment, and system service and repair. The identification of potential sources of failure will be more successful if this life cycle view of the socket is taken into consideration. It is recommended that the factors presented in this chapter be used as initial steps in the risk analysis of an IC socket technology. As information becomes available for the target application, factors can be updated and/or added.

Chapter 7: Contributions and Future Work

7.0 Contributions

This work provided a comprehensive study on the behavior of silver-filled elastomer sockets and their reliability. Previous research on this electrical contact technology had focused on physical and electrical characteristics, but only considering short-term experiments that could not obtain sufficient information for reliability modeling and life estimates. The following contributions were made by this research:

Experimentally demonstrated that industry standards, such as Telcordia GR-1217-CORE and ANSI/EIA-364, are not adequate to assess elastomer contact fitness to a given user application. It was shown that these standards can accelerate behavior that is not relevant to the operating environment.

Developed a methodology, based on the physics of failure and the Sequential Probability Ratio Test (SPRT), to estimate contact resistance and to assess its deviation from an assumed statistical distribution. The method was demonstrated for detecting changes in resistance behavior on elastomer sockets under thermal cycling conditions.

Experimentally demonstrated that the contact resistance of elastomer sockets, under mechanical load, decreases as a function of time and temperature for extended

periods of time after assembly (first year in this study), a result of increases in the effective contact area between Ag particles.

Discovered a reliability concern of assembled elastomer sockets in room temperature conditions, due to increased resistance variability over time, which can result in unacceptable increases in the probability of failure in high-density interconnects, and dead-on-arrival (DOA) systems.

Developed a quantitative reliability model for the mean contact resistance of an elastomer socket, using fundamental material properties and user-defined failure criteria.

Discovered that elastomer sockets, in spite of experiencing stress relaxation at the macroscale (elastomer), can exhibit decreases in contact resistance, a result of stress redistribution at the microscale (Ag particles), which increases Ag-Ag particle stress and the effective contact area.

7.1 Future Work

7.1.1 Socket Reliability Modeling

The research in this dissertation focused on the analysis of contact behavior and the definition of contact reliability. There is a significant amount of research that needs to be done in regards to the modeling of IC socket reliability. Current industry practices for the estimation of socket reliability consist in the application of a series or "weakest link" model, as illustrated in Figure 28.

Figure 28. Series reliability model for a system of "n" components

The series reliability model is given by

$$R_S = R_1 \cdot R_2 \cdots R_n = R^n \tag{7.1}$$

where R_s is socket reliability, R_i is reliability of a contact, and n is the number of contacts in the socket. In real applications this model provides an over-conservative estimate of socket reliability because it does not consider:

- The different contact functions on a socket (e.g. power, ground, signal)
- Innate redundancy of power and ground contacts
- Effect of contact location with respect of the package center

A socket level reliability model should consider the following:

- A contact reliability model based on the physics of failure
- Failure mechanisms specific to each contact function (e.g. AC, DC, and signal)
- Functional redundancy at package level
- Mechanical load variability effects over the surface of the package
- Contact position with respect to the package neutral point and number of contacts at that specific distance
- Clustering of failures

7.1.2 Long Term Reliability of Elastomer Sockets

The experiments in this research captured the behavior of elastomer contacts during the first year of life at nominal operating conditions. Further research is needed to model the statistical distribution shift over time, which could provide valuable information on the effects of stress relaxation during the second and third years after assembly. Since accelerating the aging of the contact by means of temperature conditions is not a feasible solution, experimental work is needed to correlate the degradation of elastomer contacts to normal operating conditions, possibly by means of power cycling and/or temperature cycling experiments.

Appendix I – Main Physical and Material Properties of the Elastomer Socket

Table 19. Main characteristics of the elastomer socket used in the research

Socket	Dimensions	53.0 x 57.0 mm (see Figure 29)
	Housing material	Thermoplastic
	Insulator material	Polyimide
	Contact count	1369 in 37 x 37 array
	Pitch	1.1 mm
	Socket stops	16 total: one on each corner plus three on each side
	Alignment posts	2
	Operating temperature range	0-90 °C
Contact	Materials	Ag particles embedded on elastomer
	Dimensions	Height: 0.90 mm (see Figure 30) Diameter: 0.51 mm Base: 0.73 mm
	Mechanical load requirements	40-80 g per contact (120 to 240 Lbs per socket)
	Maximum Deflection	0.2 mm (controlled by socket stops)
	Durability	This contact can be inserted/extracted multiple times, but re-use is not recommended due to elastomer and Ag residues left on pad upon removal (a result of contact stiction)
	Coefficient of thermal expansion (CTE)	Elastomer: 130-250 ppm for temperatures between 0 °C and 200 °C Ag: 17 ppm
	Stiffness	20-12 MPa for temperature between 0 °C and 200 °C
	Glass transition temperature (Tg)	-40 °C

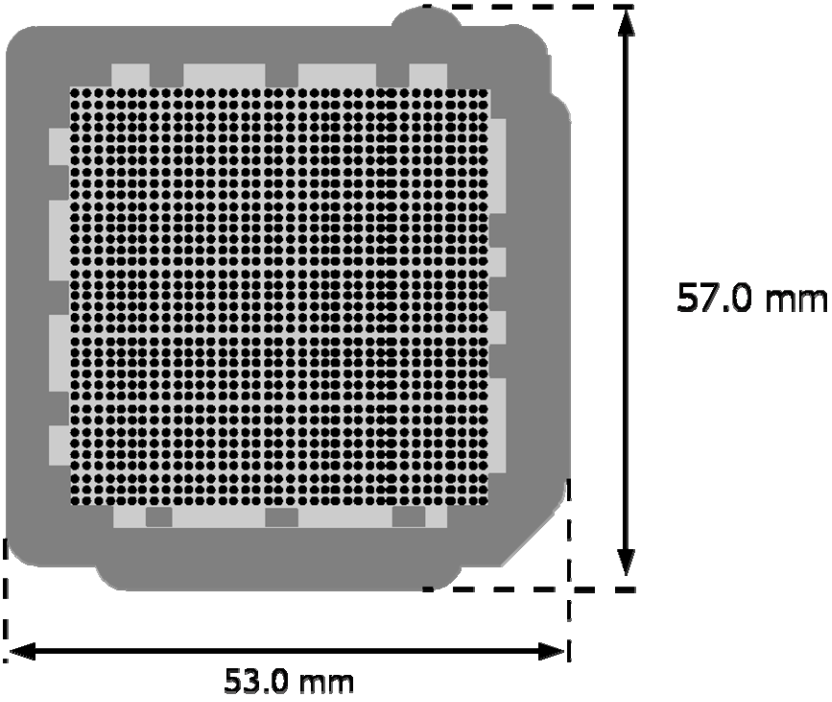

Figure 29. Illustration of elastomer socket, showing dimensions. The 37 x 37 contact array and main housing features are also shown

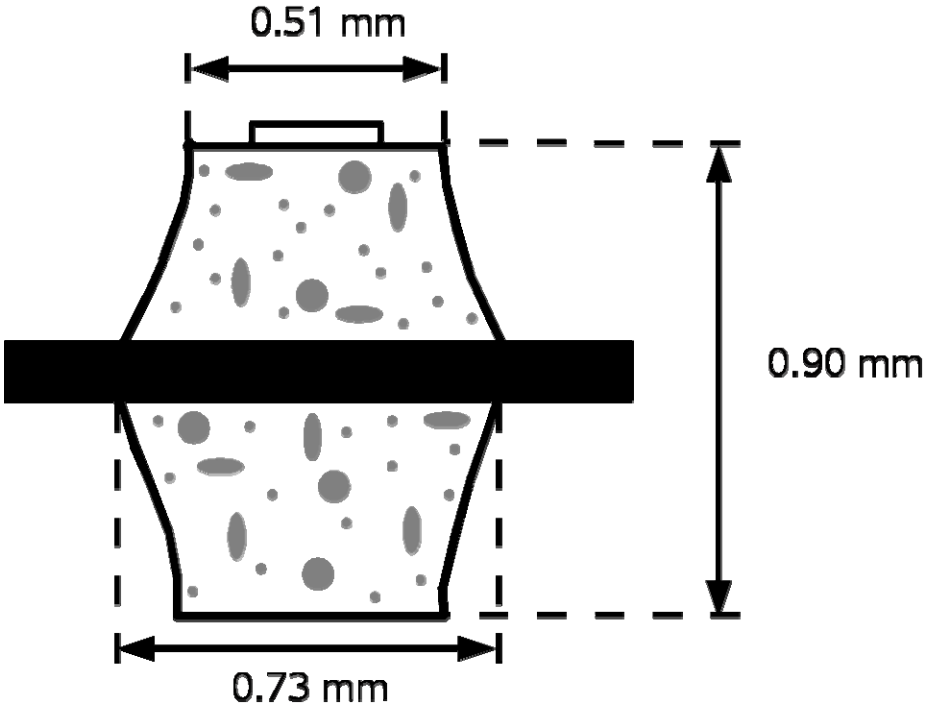

Figure 30. Illustration of elastomer contact, showing dimensions. Gray shapes inside of contact represent Ag particles. Black horizontal region at center of contact represents insulator

Appendix II – Analysis of Mechanical Load Applied to IC Socket Assemblies

Mechanical load is a key component in the operating environment of an IC socket system. If the load is too low, the socket can experience higher contact resistance values and/or intermittent failures. If the load is too high, the socket can be physically damaged. A load analysis was performed to quantify the overall applied conditions for the IC sockets that were utilized in this research.

The component thickness from 20 assembly sets (as shown in Figure 3, Chapter 2) was measured. As part of the study the constant for each one of the springs (80 springs total) was obtained by direct measurements using a force tester. The measurements provided the information needed to estimate the load that was applied by each test board assembly. The average test board load was found to be 236 Lbs., with a standard deviation of 5.7 Lbs. This translates into an average contact load of 78 g, which is within assembly requirement. The results are summarized in Table 20.

Table 20. Results of mechanical load analysis

Assembly	Total Load (Lbs)	Estimated Load per Contact (g)	Assembly	Total Load (Lbs)	Estimated Load per Contact (g)
1	232.9	77	11	247.5	82
2	238.6	79	12	237.3	79
3	231.9	77	13	238.0	79
4	232.7	77	14	233.5	77
5	234.2	78	15	226.6	75
6	234.7	78	16	244.8	81
7	230.9	77	17	233.8	77
8	230.4	76	18	233.1	77
9	245.5	81	19	243.4	81
10	236.7	78	20	242.5	80

Appendix III – Package and Bolster Plate Shape Analysis

The shape of the daisy chain packages and bolster plates that were used in this research are important factors in the load and load distribution for IC sockets. The flatness of a daisy chain package can increase or decrease the amount of load (and of contact compression) for some socket contacts. The shape of the bolster plate normalizes the load applied over the whole contact array, reducing high and low load areas. Shadow Moiré fringe analysis was used to determine the shapes of these components, allowing the rejection of samples that did not meet assembly specification. A total of 20 sets were characterized by this method, finding the mean LGA package flatness to be 3 mils, with a standard deviation of 0.4 mils. The mean bolster plate flatness was found to be 7 mils with a standard deviation of 1.2 mils. All samples were found to have acceptable parameters. Representative Shadow Moiré images are provided in Figures 31 and 32.

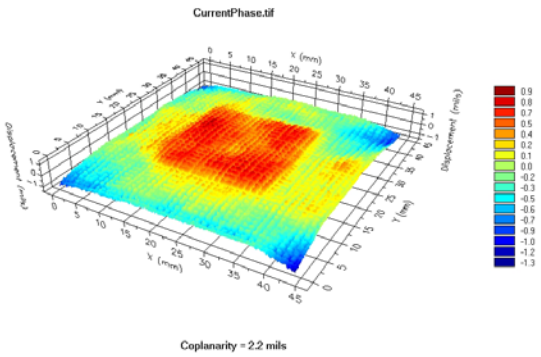

Figure 31. Shadow Moiré image for sample package

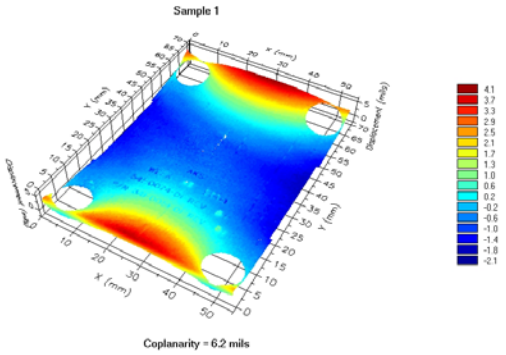

Figure 32. Shadow Moiré image for sample bolster plate

Appendix IV – Sensitivity Analysis of PoF Model Parameters and Model Accuracy Evaluation

The PoF model for the Maxima-SPRT methodology is given by (3.15)

$$R_{e'} = \frac{\rho_{T'}}{2a'}$$

where where $R_{e'}$ is estimated resistance, $\rho_{T'}$ is resistivity, and a' is a-spot radius. Both input parameters are a function of temperature T'. Resistivity, being a material property, only provides variation on the estimated resistance when the temperature of the contact changes. To assess the sensitivity of the model to changes in resistivity, the a-spot radius was set to a constant value (a-spot radius at 20 °C), and the resistance was calculated from 20 °C to 75 °C, as shown in Figure 33. A 20% increase in resistivity over temperature (from 1.63E-8 to 1.97E-8 Ω•m) resulted in a 20% increase in resistance (from 4.9 mΩ to 5.9 mΩ).

The a-spot radius contributes to variation of the estimated resistance due to changes in contact temperature and to errors from the a-spot model (goodness-of-fit of the model to actual data). To assess the sensitivity of the model to changes in a-spot radius, the resistivity was set to a constant value (resistivity at 20 °C), and the resistance was calculated from 20 °C to 75 °C, as shown in Figure 34. A 30% decrease in a-spot radius over temperature (from 1.67E-6 to 1.18E-6 Ω·m) resulted in a 40% increase in resistance (from 4.9 mΩ to 6.9 mΩ). The variability of the PoF model, resulting from a-spot radius estimation errors, was quantified by means of a repeatability study, where 25 resistance measurements were performed under

identical temperature conditions. The estimation error at a fixed temperature was found to be < 0.1 mΩ.

The model estimates were plotted against resistance measurements to validate model accuracy, as shown in Figure 35. All model estimates were found to be within 0.1 mΩ from the respective measurement.

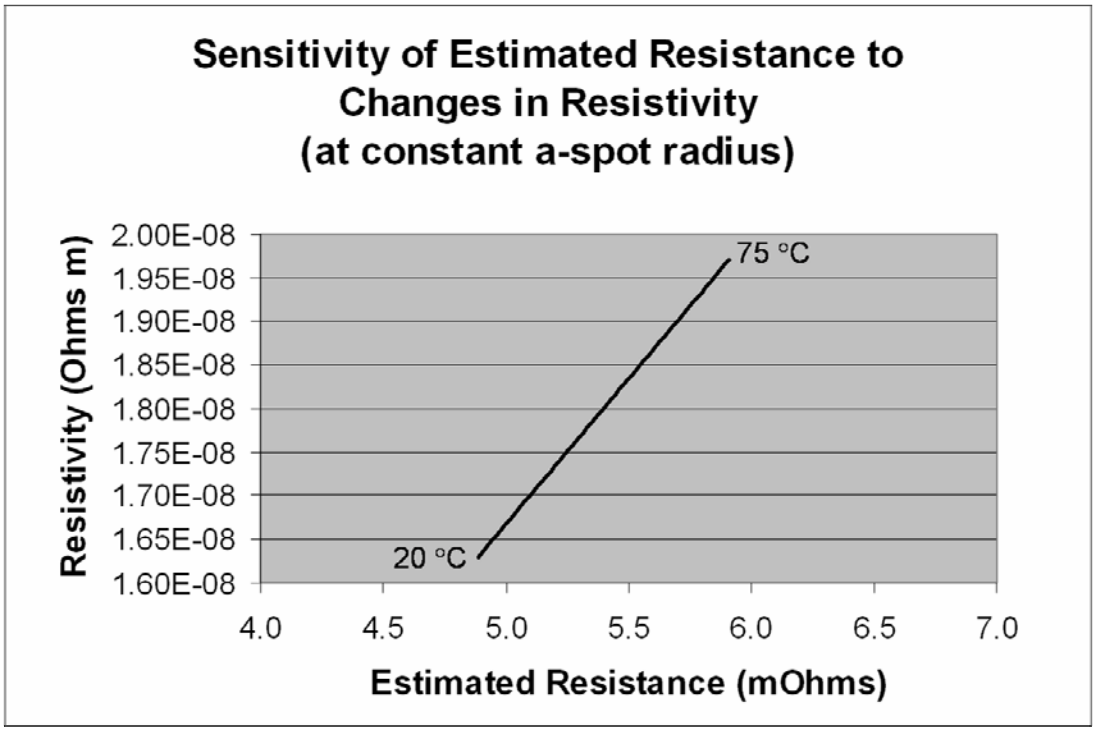

Figure 33. Sensitivity of output resistance to changes in resistivity. Resistivity is shown for 20 °C to 75 °C temperature range

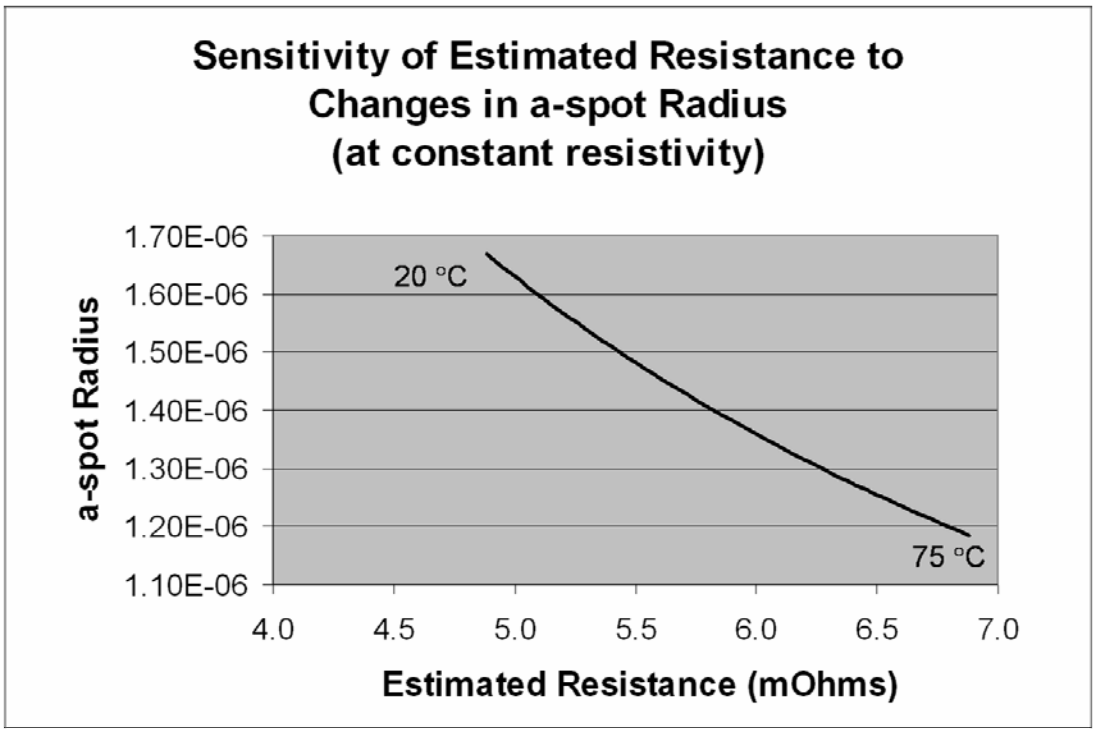

Figure 34. Sensitivity of output resistance to changes in a-spot radius. Resistivity is shown for 20 °C to 75 °C temperature range

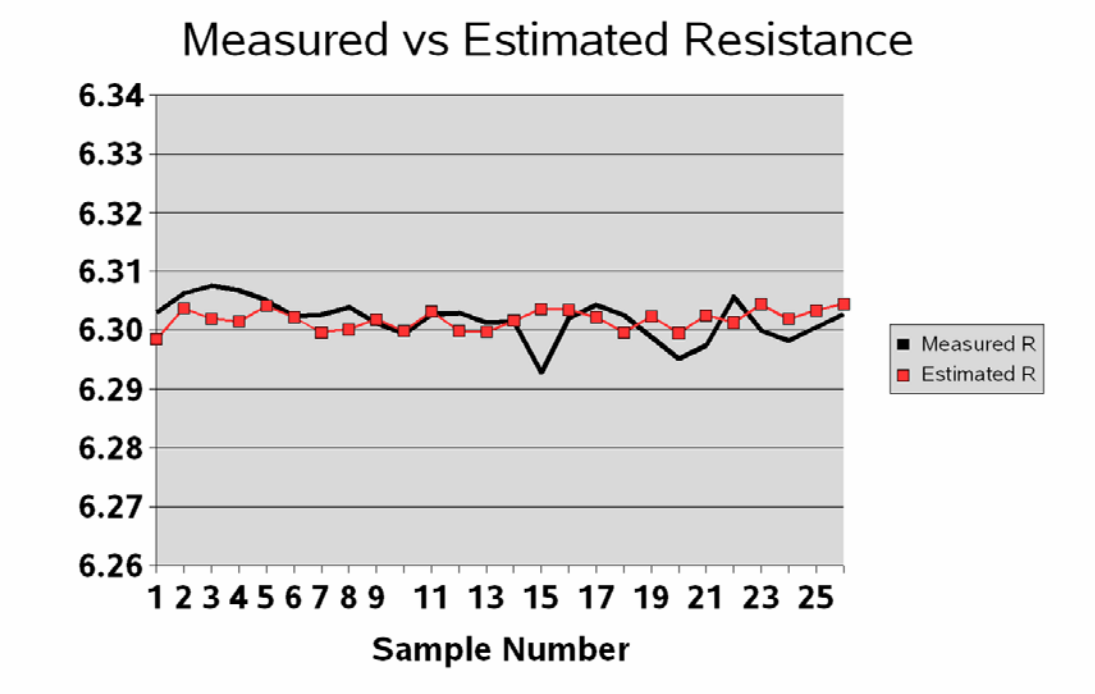

Figure 35. Plot of resistance measurements versus model estimates, validating PoF model accuracy

Appendix V – Physical Location of Test Contacts in Daisy Chain Package

The location of contacts in the daisy chain package is illustrated in Figure 36. A total of 44 contacts formed 22 daisy chains, which were located on the perimeter and center regions of the package/socket assembly.

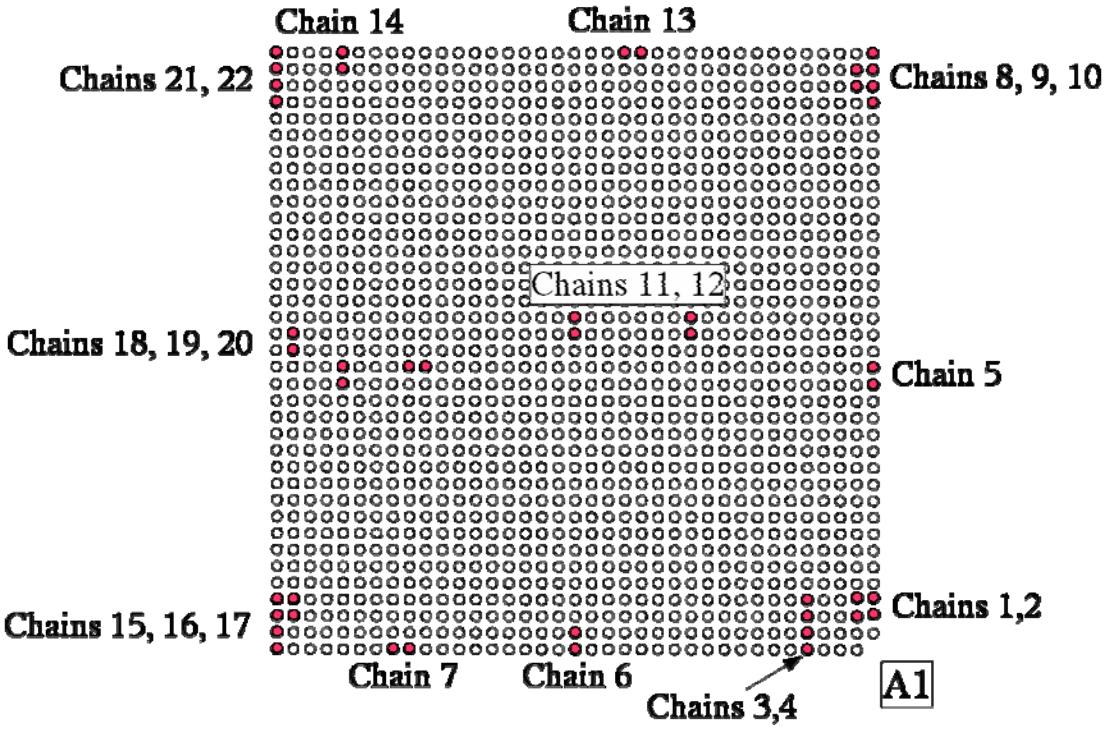

Figure 36. Illustration of the 37 x 37 array used in the experiment, showing the location of contacts that were monitored. The daisy chains are on the perimeter and center regions of the socket. Label A1 represents pin 1 corner

Appendix VI – Generalization of the PoF Model

The mean contact resistance model presented in Chapter 4 was given by

$$\mu = \frac{\rho_T}{2a} \tag{4.2}$$

$$\rho_T = \rho_{20} + \rho_{20} * (T - 293.15) * \gamma \tag{4.3}$$

where μ is estimated mean contact resistance, a is a-spot radius, ρ_T is resistivity, T is temperature in Kelvin, ρ_{20} is resistivity of Ag at 20 °C, and γ is thermal coefficient of resistivity for Ag. The a-spot radius as function of time was given by

$$a = t^m e^b \tag{4.6}$$

where t is time, m is slope, and b is intersect. A model for the a-spot was presented for each temperature condition. To provide a more general implementation, an empirical model of the a-spot radius was developed, which provided resistance estimates as a function of time *and* temperature. The empirical model is given by

$$a_{tT} = t^{m'} e^{b'} \tag{VI.1}$$

$$b' = 2.99 - 0.118 \cdot T + 0.000203 \cdot T^2 \tag{VI.2}$$

where a_{tT} is a-spot radius as a function of time and temperature, and m' is 0.085. The empirical model was evaluated using test data, finding it to provide good estimates for 25 °C, 55 °C, and 75 °C conditions. The empirical model, plotted against multiple temperatures is shown in Figure 37.

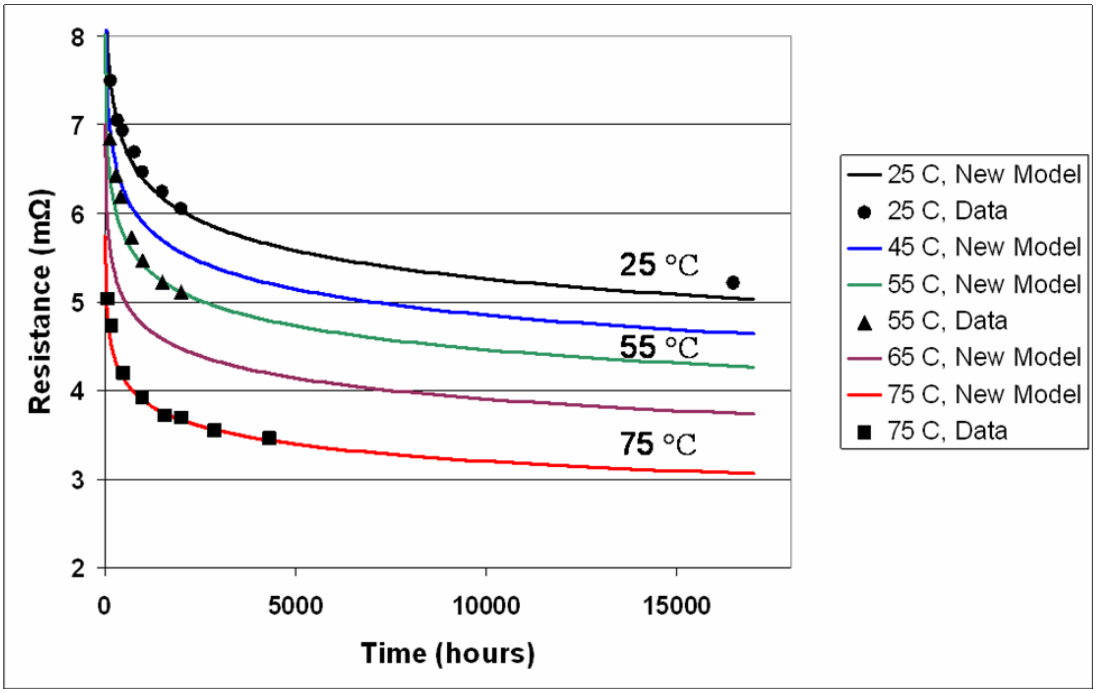

Figure 37. Plot illustrating the fit of the empirical contact resistance model against test results at 25 °C, 55 °C and 75 °C. Additional curves were created for 45 °C and 65 °C. The model provides good estimates as a function of time and temperature, with a maximum deviation of 0.1 mΩ for the 16 500 h test point at 25 °C

Bibliography

[1] Telcordia, "GR-1217-CORE, Generic Requirements for Separable Electrical Connectors Used in Telecommunications Equipment, Issue 1, Nov. 1995". Available: http://telecom-info.telcordia.com/site-cgi/ido/index.html .

[2] Electronic Industries Alliance, "ANSI/EIA-364-D-2001, Electrical Connector Socket Test Procedures Including Environmental Classifications", Virginia: EIA, 2001.

[3] D. Neidich, "cLGA® Sockets: Qualification, Production, and Performance Ready," in Proc. 27th Annual IEEE/CPMT/SEMI International Electronics Manufacturing Technology Symposium, San Jose, CA, Jul. 17-18, 2002, pp. 105-109.

[4] K. Puttlitz and P. Totta, *Area Array Interconnection Handbook*. New York: Springer-Verlag, 2001, pp. 432-434.

[5] M. Pecht, A. Shukla, N. Kelkar, and J. Pecht, "Criteria for the Assessment of Reliability Models," IEEE Transactions on Components, Packaging, and Manufacturing Technology – Part B, Vol.20, No.3, August 1997, pp. 229-234.

[6] W. Liu and M. G. Pecht, *IC Component Sockets*. New Jersey: John Wiley & Sons, Inc., 2004, pp. 21, 138-157.

[7] S. Yang, J. Wu, and M. Pecht, "Electrochemical Migration of Land Grid Array Sockets under Highly Accelerated Stress Conditions," in Proc. 51st IEEE HOLM Conference on Electrical Contacts, Chicago, IL, Sep. 26-28, 2005, pp. 238-244.

[8] N. Vichare, P. Rodgers, V. Eveloy, and M. Pecht, "In Situ Temperature Measurements of a Notebook Computer – A Case Study in Health and Usage Monitoring of Electronics," IEEE Transactions on Device and Materials Reliability, Vol.4, No.4, December 2004, pp. 658-663.

[9] L. Lopez, S. Nathan, and S. Santos, "Preparation of Loading Information for Reliability Simulation," IEEE Transactions on Components and Packaging Technologies, Vol.27, No.4, December 2004, pp. 732-735.

[10] L. Lopez and S. Nathan, "Virtual Qualification of IC Sockets Using Probabilistic Engineering Methods," in Proc. Annual Reliability and Maintainability Symposium, Orlando, FL, Jan. 22-25, 2007, pp. 271-276.

[11] L. Lopez, "Advanced Electronic Prognostics Through System Telemetry and Pattern Recognition Methods," Microelectronics Reliability, Vol. 47, No.12, December 2007, pp 1865-1873.

[12] L. Lopez and M. Pecht, "Maxima-SPRT Methodology for Health Monitoring of Contact Resistance in IC Sockets," in Proc. International Conference on Prognostics and Health Management, Denver, CO, October 6-9, 2008.

[13] K. Whisnant, K. Gross, and N. Lingurovska, "Proactive Fault Monitoring in Enterprise Servers," in Proc. IEEE International Multiconference in Computer Science and Computer Engineering, Las Vegas, NV, June 27-30, 2005, pp. 3-10.

[14] Y. Lam, C. Maul, and J. McBride, "Temperature, Humidity and Pressure Measurement on Automotive Connectors," IEEE Transactions on Components and Packaging Technologies, Vol.29, Issue 2, June 2006, pp. 333-340.

[15] R. Holm, *Electric Contacts, Theory and Applications*. New York: Springer, 2000, pp. 114-116.

[16] K. Whisnant, R. Dhanekula, and K. Gross, "Efficient Signal Selection for Nonlinear System-Based Models of Enterprise Servers," in Proc. Third IEEE International Workshop on Engineering of Autonomic & Autonomous Systems (EASe'06), Potsdam, Germany, March 27-30, 2006, pp. 141-148.

[17] K. Vaidyanathan, K. Gross, and R. Dhanekula, "Incipient Fault Detection in Storage Systems Using On-line Pattern Recognition," in Proc. Machinery Failure Prevention Technology Conference (MFPT-60), Virginia Beach, VA, April 26-30, 2006, pp. 101-110.

[18] R. Schmidth and H. Shaukatullah, "Computer and Telecommunications Equipment Room Cooling: A Review of Literature," IEEE Transactions on Components and Packaging Technologies, Vol.26, No.1, March 2003, pp. 89-98.

[19] L. Lopez and M. Pecht, "Assessing the Operating Temperature and Relative Humidity Environment of IC Sockets in Enterprise Servers," in Proc. International Conference on Prognostics and Health Management, Denver, CO, October 6-9, 2008.

[20] J. Xie, C. Hillman, P. Sandborn, M. Pecht, A. Hassanzadeh, and D. DeDonato, "Assessing the Operating Reliability of Land Grid Array Elastomer Sockets," IEEE Transactions on Components and Packaging Technologies, vol. 23, no. 1, pp. 171-176, Mar. 2000.

[21] W. Liu, M. G. Pecht, and J. Xie, "Fundamental Reliability Issues Associated with a Commercial Particle-in-Elastomer Interconnection System," IEEE Transactions on Components and Packaging Technologies, vol. 24, no. 3, pp. 520-525, Sep. 2001.

[22] J. Hofmeister, P. Lall, D. Goodman, E. Ortiz, M. Adams, and T. Tracy, "Intermittency Detection and Mitigation in Ball Grid Array (BGA) Packages,"

[23] M. G. Pecht, *Prognostics and Health Management of Electronics*. New York: John Wiley & Sons, Inc., 2008.

[24] Electronic Industries Alliance, "EIA/ECA-364-23C, Low Level Contact Resistance Test Procedure for Electrical Connectors and Sockets," Virginia: EIA, 2006.

[25] H. Qi, N. Vichare, M. Azarian, and M. G. Pecht, "Analysis of Solder Joint Failure Criteria and Measurement Techniques in the Qualification of Electronic Products," IEEE Transactions on Components and Packaging Technologies, vol. 31, no. 2, pp. 469-477, Jun. 2008.

[26] P. Lall, M. G. Pecht, and E. Hakim, *Influence of Temperature on Microelectronics and System Reliability: A Physics of Failure Approach*. New York: CRC Press LLC, 1997, pp. 12.

[27] P. Tobias and D. Trindade, *Applied Reliability*. New York: Chapman & Hall/CRC Press, 1998, pp. 187.

[28] J.A. Fulton, D. Horton, R. Moore, W. Lambert, S. Jin, R. Opila, R. Sherwood, T. Tiefel, and J. Mottine, "Electrical and Mechanical Properties of a Metal-Filled Polymer Composite for Interconnection and Testing Applications," in Proc. 39th Electronic Components Conference, Houston, TX, May 22-24, 1989, pp. 71-77.

[29] N. Tunca and G. Rosen, "Environmental Testing of Elastomer Connectors," In Proc. 38th IEEE HOLM Conference on Electrical Contacts, Chicago, IL, Oct. 18-21, 1992, pp. 249-255.

[30] K. Kim, J. Kim, S. Kim, K. Lee, A. Chen, N. Ahmad, N. Dugbartey, M. Karnezos, S. Tam, Y. Kweon, and R. Pendse, "The Viability of Anisotropic Conductive Film (ACF) as a Flip Chip Interconnection Technology," In Proc. 50th Electronic Components and Technology Conference, Las Vegas, NV, May 21-24, 2000, pp. 1122-1132.

[31] H. Kristiansen and J. Liu, "Overview of Conductive Adhesive Interconnection Technologies for LCD's," IEEE Transactions on Components, Packaging, and Manufacturing Technology – Part A, vol. 21, no. 2, pp. 208-214, Jun. 1998.

[32] S. Mannan, D. Williams, and D. Whalley, "Some Optimum Processing Properties for Anisotropic Conductive Adhesives for Flip Chip Interconnector," Journal of Materials Science: Materials in Electronics, vol.8, no.4, pp. 223-231, Aug. 1997.

[33] K. Keswick, R. German, M. Breen, and R. Nolan, "Compliant Bumps for Adhesive Flip-Chip Assembly," IEEE Transactions on Components, Packaging, and Manufacturing Technology – Part B, vol. 18, no. 3, pp. 503-510, Aug. 1995.

[34] D. Chang, P. Crawford, J. Fulton, R. McBride, M. Schmidt, R. Sinitski, and C. Wong, "An Overview and Evaluation of Anisotropically Conductive Adhesive Films for Fine Pitch Electronic Assembly," IEEE Transactions on Components, Hybrids, and Manufacturing Technology, vol. 16, no.8, pp. 828-835, Dec. 1993.

[35] M. Mundlein and J. Nicolics, "Electrical Resistance Modeling of Isotropically Conductive Adhesive Joints," In Proc. 28th International Spring Seminar on Electronics Technology, Wiener Neustadt, Austria, May. 19-22, 2005, pp. 128-133.

[36] M. Brumbach and J. Nadon, *Industrial Electricity*, 7th Edition. New York: Thomson/Del Mar Learning, 2005, pp. 157.

[37] A. Clauset, C. Shalizi, and M. Newman. (2007, June). Power-law Distributions in Empirical Data. ArXiv eprint. Volume 706, Available: http://arxiv.org/abs/0706.1062

[38] L. Lopez, V. Challa, and M. Pecht, "Assessing the Reliability of Elastomer Sockets in Temperature Environments," IEEE Transactions on Device and Materials Reliability, vol. 9, no. 1, pp. 80-86, March 2009.

[39] M. J. Nicolics, "Electrical Resistance Modeling of Isotropically Conductive Adhesive Joints," In Proc. 28th International Spring Seminar on Electronics Technology, Wiener Neustadt, Austria, May. 19-22, 2005, pp. 128-133.

[40] P. S. Slade, *Electrical Contacts: Principles and Applications*. New York: Marcel-Dekker, Inc., 1999, pp. 1-14.

[41] W. Liu, M. Lee, M. Pecht, and R. Martens, "An Investigation of the Contact Resistance of a Commercial Elastomer Interconnect Under Thermal and Mechanical Stresses," IEEE Transactions on Device and Materials Reliability, vol. 3, no. 2, pp. 39-43, Jun. 2003.

[42] S. Yang, J. Wu, D. Tsai, and M. G. Pecht, "Contact Resistance Estimation for Time-Dependent Silicone Elastomer Matrix of Land Grid Array Socket," IEEE Transactions on Components and Packaging Technologies, vol. 30, no. 1, pp. 81-85, Mar. 2007.

[43] J. Xie, M. Pecht, D. DeDonato, and A. Hassanzadeh, "An Investigation of the Mechanical Behavior of Conductive Elastomer Interconnects," Microelectronics Reliability, vol. 41, no. 2, pp. 281-286, Dec. 2001.

[44] W. Liu, "Reliability Assessment of Metal Particle-in-Elastomer Sockets," Ph.D. dissertation, Dept. Mech. Eng., University of Maryland, College Park, MD, 2001.

[45] W. Meeker and L. Escobar, *Statistical Methods for Reliability Data*. New York: Wiley Inter-science, 1998, pp. 475.

[46] W. Nelson, *Accelerated Testing: Statistical Models, Test Plans, and Data Analysis*. New York: Wiley, 2004, pp. 79-82.

[47] R. L. Edgeman, "Assessing the Inverse Gaussian Distribution," IEEE Transactions on Reliability, vol. 39, no. 3, pp. 353-355, Aug. 1990.

[48] R. S. Chhikara and L. Folks, *The Inverse Gaussian Distribution: Theory, Methodology, and Applications*. New York: Marcel-Dekker Inc., 1989, pp. 71-74.

[49] National Institute of Standards and Technology, "Engineering Statistics Handbook". Available: http://www.itl.nist.gov/div898/handbook/eda/section3/eda35g.htm.

[50] D. Kececioglu, *Reliability and Life Testing Handbook. Pennsylvania*: DESTech Publications, 2002, pp. 725-728.

[51] M. Brumbach and J. Nadon, *Industrial Electricity, 7th Edition*. New York: Thomson/Del Mar Learning, 2005, pp. 157.

[52] R. Mroczkowski and J. Maynard, "Estimating the Reliability of Electrical Connectors," IEEE Transactions on Reliability, Vol.40, No.5, December 1991, pp. 507-512.

[53] R. Mroczkowski, "Concerning Reliability Modeling of Connectors," in Proc. 54th IEEE HOLM Conference on Electrical Contacts, Arlington, VA, Oct. 26-28, 1998, pp. 57-68.

[54] R. Timsit, "Electrical Conduction Through Small Contact Spots," IEEE Transactions on Components and Packaging Technologies, Vol.29, No.4, December 2006, pp. 727-734.

[55] D. Harris and M. Pecht, "A Reliability Study of Fuzz Button Interconnects," Microelectronics Reliability, Vol.36, No.4, April 1996, pp. 550-557.

[56] M. Modarres, M. Kaminskiy, and V. Krivtsov, *Reliability Engineering and Risk Analysis, A Practical Guide*. New York: Marcel/Dekker, Inc., 1999, pp. 408.